รายงานวิจัยฉบับสมบูรณ์

โครงการ การพัฒนาวัสดุโครงสร้างประกอบระหว่างวัสดุแม่เหล็กและวัสดุกึ่งตัวนำอินทรีย์สำหรับการประยุกต์ในอุปกรณ์สปินอิเล็กทรอนิกส์

โดย ดร.อัศวิน สินทรัพย์

สิงหาคม 2563

สัญญาเลขที่ MRG5380127

รายงานวิจัยฉบับสมบูรณ์

โครงการ การพัฒนาวัสดุโครงสร้างประกอบระหว่างวัสดุแม่เหล็กและวัสดุกึ่งตัวนำอินทรีย์สำหรับการประยุกต์ในอุปกรณ์สปินอิเล็กทรอนิกส์

ดร. อัศวิน สินทรัพย์

ภาควิชาฟิสิกส์ คณะวิทยาศาสตร์ มหาวิทยาลัยมหิดล

สนับสนุนโดยสำนักงานคณะกรรมการการอุดมศึกษา สำนักงานกองทุนสนับสนุนการวิจัย และมหาวิทยาลัยมหิดล

บทคัดย่อ

รหัสโครงการ: MRG5380127

ชื่อโครงการ: การพัฒนาวัสดุโครงสร้างประกอบระหว่างวัสดุแม่เหล็กและวัสดุกึ่งตัวนำอินทรีย์สำหรับการประยุกต์ในอุปกรณ์สปินอิเล็กทรอนิกส์

ชื่อนักวิจัย และสถาบัน: อัศวิน สินทรัพย์ คณะวิทยาศาสตร์ มหาวิทยาลัยมหิดล

Email address: asawin.sin@mahidol.ac.th

ระยะเวลาโครงการ: 2 ปี

งานวิจัยนี้เป็นการศึกษาหาเงื่อนไขที่เหมาะสมในการผลิตวัสดุโครงสร้างประกอบระหว่างวัสดุกึ่งตัวนำอินทรีย์กับวัสดุแม่เหล็กด้วยวิธีการที่มีค่าใช้จ่ายต่ำแต่ได้คุณสมบัติทางแม่เหล็กและคุณสมบัติเกี่ยวกับการขนส่งสปินของอิเล็กตรอนที่เหมาะสมกับการใช้งานเป็นอุปกรณ์สปินอิเล็กทรอนิกส์ ในส่วนของวัสดุแม่เหล็กได้มีการศึกษาหาปัจจัยที่เหมาะสมในการผลิตฟิล์มบางอัลลอยของเหล็กและนิกเกิลโดยวิธีการสะสมทางไฟฟ้า โดยปัจจัยที่ทำการศึกษาประกอบด้วยความเข้มข้นของไอออนเหล็กและนิกเกิลในสารละลาย ปริมาณสารเติมแต่งและการใช้สนามแม่เหล็กภายนอกร่วมระหว่างการผลิตฟิล์ม นอกจากนี้ยังมีการศึกษาการผสมอะตอมที่มีคุณสมบัติแม่เหล็กเพิ่มเติมเพื่อผลิตเป็นฟิล์มบางอัลลอยของสามโลหะที่มีคุณสมบัติทางแม่เหล็กตามที่ต้องการได้ รวมทั้งมีการศึกษาการใช้กรรมวิธีทางความร้อนกับวัสดุอัลลอยที่ได้เพื่อสร้างวัสดุแม่เหล็กประเภทออกไซด์ซึ่งมีคุณสมบัติทางไฟฟ้าและทางแม่เหล็กแตกต่างไปจากวัสดุเดิมได้ สำหรับส่วนของวัสดุกึ่งตัวนำอินทรีย์ได้มีการศึกษาหาปัจจัยที่เหมาะสมในการผลิตฟิล์มบางสารกลุ่มฟทาโลไซยานีนซึ่งมีโลหะเป็นอะตอมกลาง (MPc) เช่น NiPc CoPc FePc และ CuPc เป็นต้น โดยใช้วิธีสองวิธีคือ วิธีการสะสมในสุญญากาศ และ การเกาะติดแบบชั้นต่อชั้น ในการวิจัยนี้ยังมีการพัฒนาสร้างระบบวัดปรากฏการทัศนศาสตร์เชิงแสงแบบเคอร์ (MOKE) เพื่อใช้ศึกษาคุณสมบัติเชิงแม่เหล็กและคุณสมบัติที่เกี่ยวเนื่องกับการขนส่งสปิน ในวัสดุแม่เหล็ก วัสดุอินทรีย์ และ วัสดุโครงสร้างประกอบระหว่างวัสดุทั้งสอง ระบบวัดที่สร้างขึ้นนี้สามารถวัดคุณสมบัติทางแม่เหล็กของฟิล์มบางสารกลุ่มฟทาโลไซยานีนซึ่งมีโลหะเป็นอะตอมกลางที่ผลิตขึ้นได้อย่างได้ผลดีกว่าวิธีอื่นที่มีอยู่ในห้องปฏิบัติการ อย่างไรก็ตามผลการศึกษาคุณสมบัติของวัสดุโครงสร้างประกอบระหว่างวัสดุกึ่งตัวนำอินทรีย์กับวัสดุแม่เหล็กที่ผลิตได้พบว่ายังต้องการการปรับปรุงปัจจัยการผลิตเพิ่มเติมเพื่อให้ได้วัสดุโครงสร้างประกอบที่เหมาะสมกับการใช้งานเป็นอุปกรณ์สปินอิเล็กทรอนิกส์

คำหลัก: วัสดุโครงสร้างประกอบ ฟิล์มบางแม่เหล็ก สารกึ่งตัวนำอินทรีย์ ทัศนศาสตร์แม่เหล็ก

Abstract

Project Code: MRG5380127

Project Title: **Development of organic-semiconductor/magnetic heterostructures for spin-electronic devices**

Investigator: Asawin Sinsarp, Faculty of Science, Mahidol University

Email address: asawin.sin@mahidol.ac.th

Project Period: 2 years

The fundamental studies being necessary for constructing low-cost organic-semiconductor/magnetic heterostructures with appropriate magnetic and spin transport properties were done. For magnetic material part, the conditions for preparing iron-nickel alloy thin films by electrodeposition were optimized. Various conditions, such as the concentrations of iron and nickel ions in electrolytes, the amounts of additives in electrolytes, the in-situ applied magnetic field, were studied. The mixing of other kinds of magnetic atoms such as cobalt atoms to the iron and nickel atoms to form tertiary magnetic metal alloys with tunable magnetic properties were also studied. Heat treatment of the obtained magnetic materials to form magnetic metal oxides as another class of magnetic materials were also studied. For organic-semiconductor part, the conditions for preparing metal-phthalocyanine (MPc)-based thin films such as NiPc, CoPc, FePc, CuPc were studied using two method: vacuum deposition and layer-by-layer formation in solutions. The magneto-optical Kerr effect (MOKE) measurement system was developed to measure the magnetic and spin-related properties of metal and organic thin films, as well as their heterostructures. The MOKE measurement system was used to investigate the magnetic properties of various metal-phthalocyanine (MPc)-based thin films such as NiPc, CoPc, FePc, CuPc. In spite of the fact that all MPc-based thin films used in our studies cannot be measured by the VSM, our MOKE measurement system is sensitive enough to measure the magnetic properties of the films. The results of the studies also showed that the conditions

for preparing the organic-semiconductor/magnetic heterostructures need to be improved in order to be suitable for the application as spin-electronic devices.

Keywords: heterostructure, magnetic thin film, organic semiconductor, magneto-optics

Executive Summary

The basic studies to find the conditions suitable for constructing low-cost organic-semiconductor/magnetic heterostructures with appropriate magnetic and spin transport properties were done. The suitable condition for the preparation of Fe-Ni alloy thin film by electrodepoisition were studied. The properties of Fe-Ni alloy depend on the composition of iron and nickel. These can be caused by many conditions such as variation of metal ions in the electrolyte, additive, external magnetic field. The main works of this thesis are consisted of 2 parts. The first part is the preparation of Fe-Ni alloy thin films and the second part is the characterization of thin film.

The preparation of Fe-Ni thin film is very important because the main properties of alloy thin films are affected by the structure of alloy thin film. Many researchers reported the preparation of Fe-Ni alloy with many methods. The electrodeoposition is favor to study because this method allows for the mass production of metal alloy at low cost and can control the structure of thin film. The conditions studied in this project includes the variation of iron and nickel ion in the electrolyte, the additive to the electrolyte, external magnetic field during preparation and in-situ electrochemical cell for monitoring the initiation of Fe-Ni alloy thin film. The Fe-Ni alloy thin films are characterized by X-ray diffraction to explain the crystal structure of alloy thin films. Flame atomic absorption spectroscopy (FAAS), X-ray absorption spectroscopy (XAS) and time-resolved X-ray absorption spectroscopy (TRXAS) are used for investigate the properties of Fe-Ni alloy thin film.

The structure of Fe-Ni alloy thin films were investigated by X-ray diffraction (XRD). The XRD patterns can be observed 2 peaks to identify the structure of iron and nickel. The 1st peak shows the intensity peak around value of 2θ as 45^{o} and another peak shows at 51^{o} to 52^{o} of diffraction angle (2θ). The results show that the first peak is consisted by 2 crystalline orientation including BCC (110) and FCC (111). It can be confirmed by the XRD

pattern of nickel thin film that can observe only FCC (111) crystalline orientation. XRD pattern of nickel thin film is compared with another composition of iron and nickel ions. The 1st peak usually shows the broad peak because the combination of BCC (110) and FCC (111) crystalline orientation. In addition, the 2nd peak can be indicated FCC (200) crystalline orientation. However, these results show the effect of saccharin when add into the electrolyte. The results show the saccharin affect to increase iron content in Fe-Ni thin films but the structure is similarly to without saccharin addition. It can be concluded that the structure of Fe-Ni alloy thin film is mixture phase with BCC and FCC. So, these results have to compare with XAS and the simulation to describe the exactly crystal structure of thin film.

For investigation of the effect of applied magnetic field during the deposition on the thin film properties, it can be observed that the FCC structure and BCC structure is reduced by applying magnetic field at the cathode. The magnet field may oppose the initiation of iron films. However, the magnetic field has little effect to crystallinity of nickel films.

The magneto-optical Kerr effect (MOKE) measurement system was developed for investigating the magnetic properties of metal and organic thin films. The MOKE measurement setup consists of a laser as a light source, polarizers, a source of magnetic field, a photoelastic modulator (PEM), a lock-in amplifier and a photodetector. The MOKE measurement is carried out based on the technique of polarization modulation using the PEM and lock-in detection technique using the lock-in amplifier. The MOKE measurement setup can be operated in both longitudinal and polar modes. One of two types of magnetic field sources – copper-coil electromagnet and movable permanent magnet was used in the system. The home-made electromagnet is made of a copper coil with the resistance of 70.4 Ω. It produces a magnetic field of 107 mT at the maximum current of 2.84 A, which is in good agreement with the value of 113 mT calculated theoretically using equation (3.2).

However, the disadvantage of using this home-made electromagnet is the instability of the magnetic field due to the resistive heating in the coil. On the other hand, the movable permanent magnet uses the NdFeB magnet bar with the surface area of 5×5 cm^2 and the thickness of 2 cm. The magnet is equipped with the mechanism moving along a straight line approaching to or releasing from the sample holder to vary the magnetic field. The maximum magnetic field of 170 mT can be applied to the sample when the magnet surface is 10 mm apart. However, the disadvantage of using this movable permanent magnet is the instability of the magnetic field resulted from the vibration due to the driving mechanism.

The MOKE measurement setup was tested by measuring the magnetic properties of an electrodeposited nickel (Ni) thin film. The results of the MOKE measurement in both longitudinal and polar modes show that the magnetization of the sample along the out-of-plane direction is easier than that of the in-plane direction. It implies that this electrodeposited Ni film preferred (111) orientation since the magnetic-easy axis of the bulk Ni crystal is along the [1,1,1] direction. These MOKE results are in good agreement with the results measured using the home-built vibrating-sample magnetometer. The performance of the developed MOKE measurement setup has been verified.

The MOKE measurement of various organic thin films such as metal tetrasulphonated phthalocyanine (MTsPc, M = Fe, Ni and Cu) and metal phthalocyanine (MPc, M = Fe, Co and Cu) thin films were investigated. The MTsPc thin films were prepared by layer-by-layer technique as multi-PAH/MTsPc-bi-layer thin film on glass substrates. The MPc thin films were prepared on glass substrates by thermal evaporation under vacuum. For all kinds of the thin films, the Kerr signal of each film increases linearly with applied magnetic field. The Kerr signal of the FeTsPc thin film is strongest among three kinds of MTsPc thin films. For MPc thin films, the Kerr signal of the FePc and the CoPc thin films are comparably strong and are stronger than that of the CuPc thin film. Nonetheless, the magnetic properties of these films cannot be measured using the home-built VSM due to their small magnetization as usually for the case of organic compounds. The results indicate that the developed MOKE

measurement system is suitable for measuring the magnetic properties of organic-compound thin films. However, the results of the studies also showed that the conditions for preparing the organic-semiconductor/magnetic heterostructures need to be improved in order to be suitable for the application as spin-electronic devices.

เนื้อหางานวิจัย

1. Introduction

Spintronics is a field of research that combines the electron spin properties with the electron charge properties used in conventional electronic devices. This resulted in a new line of devices with high efficiency, high sensitivity and low power consumption. In general, electronic spin devices are based on the electron spin properties obtained by the use of magnetic materials to form a structure in conjunction with semiconductor materials used in conventional electronic devices. It requires modern methods and expensive tools. Using magnetic materials in conjunction with organic semiconductor materials, which have lower production costs than conventional semiconductors, give an opportunity to produce a new line of electronic devices called "organic spintronics", with high-performance but low-cost. [1], [2] It is considered to be suitable for the economic conditions of developing countries.

Organic spintronic equipment requires a composite structure between magnetic materials and organic-semiconductor materials that can maintain the electron spin properties when electrons are transported from the magnetic structure to the organic semiconductor materials. Therefore, the development of composite structures between magnetic materials and organic-semiconductor materials with appropriate and controllable interface properties is important to produce efficient organic spintronics equipment. In this research, conditions to prepare good but inexpensive magnetic materials, organic materials, and their composite structure were studied. In addition, the magneto-optics measurement system was developed to investigate the spin properties of the materials. [3]

2. Iron-nickel alloy thin films prepared by electrodeposition

a. Introduction

Iron-nickel (Fe-Ni) alloy is a useful magnetic material widely used in spintronics application. The variation of composition is used to tune the properties of the Fe-Ni alloy. In this part of research, the suitable conditions for the preparation of the Fe-Ni alloy thin films with tunable composition by electrodeposition method were studied. Various conditions in the studies include the amount of iron and nickel ions in electrolyte, amount of additives in electrolyte, applying an external magnetic field during preparation and types of an in-situ electrochemical cell. The crystal structure of Fe-Ni alloy thin films is determined by X-ray diffraction (XRD) analyses. X-ray absorption spectroscopy (XAS) is used to investigate the amount of Fe-Ni metal in alloy thin films. The initiate of deposition of Fe-Ni alloy thin films are described by the oxidation state of iron and nickel ions measured by time-resolved X-ray absorption spectroscopy (TRXAS).

b. Preparation of Fe-Ni alloy thin films

the compositions of nickel and iron ions in electrolyte are varied including 100:0, 85:15, 75:25, 65:35 50:50, 35:65, 25:75, 15:85 and 0:100 by varying the ratio of Ni(II)SO_4 and Fe(II)SO_4 in solutions. All chemicals are dissolved with DI water. Boric acid, Na_2SO_4 and saccharin are added to the solutions, and the pH is adjusted to be 2.0 by 1 M HCl. The alloy thin films are electro-deposited at the current density value of 4 mA/cm^2 for 2 minutes at room temperature with no agitation. The schematic picture of the Fe-Ni alloy electrodeposition is shown in Figure 2.1. The effect of magnetic field on the formation of the Fe-Ni thin film was studied by placing the permanent magnet close to the anode (MA) or cathode (MC), as schematically shown in Figure 2.2.

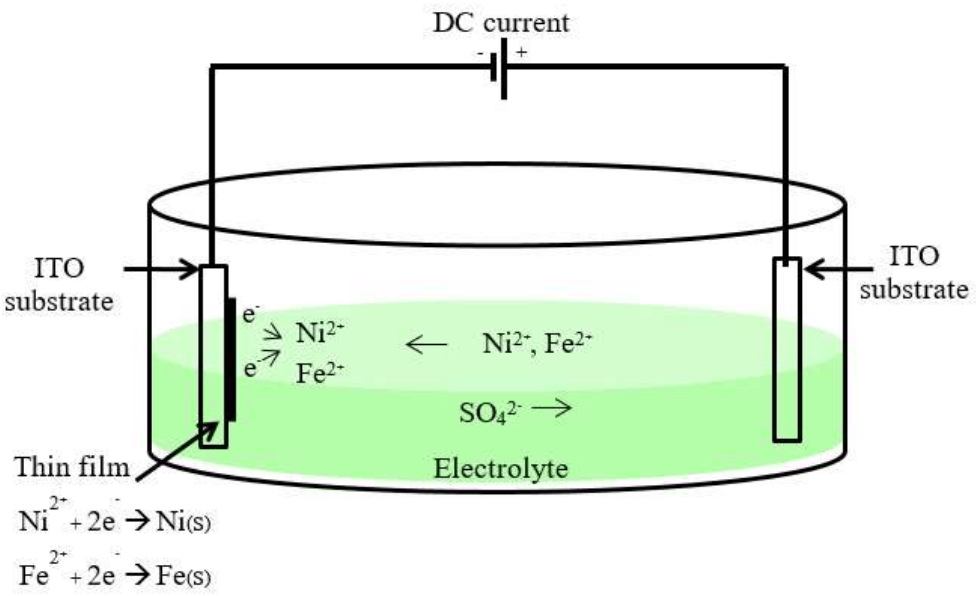

Figure 2.1 Schematic picture of iron-nickel thin film fabrication by electrodeposition method is shown.

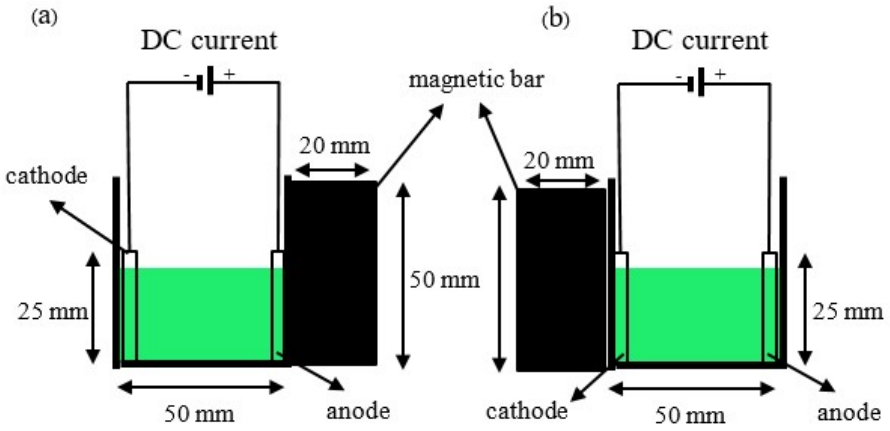

Figure 2.2 The schematic picture shows the setting for the study of the effect of magnetic field on the formation of the Fe-Ni thin film. The permanent magnet is placed (a) close to the anode (MA) and (b) close to the cathode (MC).

c. Variation of iron and nickel ions in the electrolyte with and without additive

Fe-Ni alloy thin films are prepared by elecrodeposition with various composition of iron and nickel ion. Metal alloy thin films are growth on ITO coated glass. All of thin films are characterized by X-ray diffraction with Cu-K$\propto$ radiation (λ=1.54 Å). In addition, Fe-Ni alloy thin films were investigated by many researchers. They found the crystal structure of this alloy was determined by 3 important peaks. 2 of important peaks displayed value of 2θ around 45^0. This diffraction angle represented BCC (110) [4] and FCC (111) [5]–[7] crystalline orientation in film growth direction. Last important peak was observed around 51^0 to 52^0. This peak determined the FCC (200) orientation [6]. Some researchers explained FCC (200) orientation for value of 2θ as 51^0 that showed the properties of NiFe FCC phase [4]–[6]. However, the diffraction peak at 52^0 was observed with nickel thin film [8]. When comparing the results in two trends that could observe, we can conclude that the diffraction pattern displayed the diffraction peak at 2θ as 51^0 because of the NiFe FCC phase. If pure nickel ions solutions were added by iron ions, the Fe-Ni thin film would show the diffraction peak at 51° because the size of iron in the structure would increase the lattice constant. For pure nickel ion [8], the XRD pattern show the diffraction at 52^0. It can be implied that the structure of Fe-Ni alloy can be identified by 3 base peaks and the 3rd peak at 2θ as 51 to 52° can use for describe the structure of Fe-Ni alloy thin films.

The Fe-Ni alloy thin films are prepared by electrodeposition without saccharin in the electrolyte as report in Figure 2.3 (a). The results show the X-ray diffraction patterns with some peaks. The diffraction peak displays the diffraction angle around 45°, 51° and 52°. From the literature, 1st peak can be identified BCC (110) and FCC (111) crystalline orientation. In addition, the diffraction angle around 51° and 52° use for identify FCC (200) crystalline orientation. The relationship between lattice constant and percentage of iron ions in electrolytes are displayed in Figure 2.4 (a), (b) and (c). The XRD patterns show the different

results with addition of saccharin. The 1st peak of Fe-Ni alloy thin film is evident at 45^0 this angle represents the combination of diffraction peak from BCC (110) and FCC (111). In this results, the diffraction angle of Fe 0 (Ni 100) can be represented FCC (111) that separate from combination of 1st peak when compare with another composition of iron and nickel ions. These results display the combination of diffraction from BCC and FCC structure in Fe 25, Fe 50 and Fe 75. In addition, XRD pattern of Fe 0 shows sharp peak that can represent crystalinity structure.

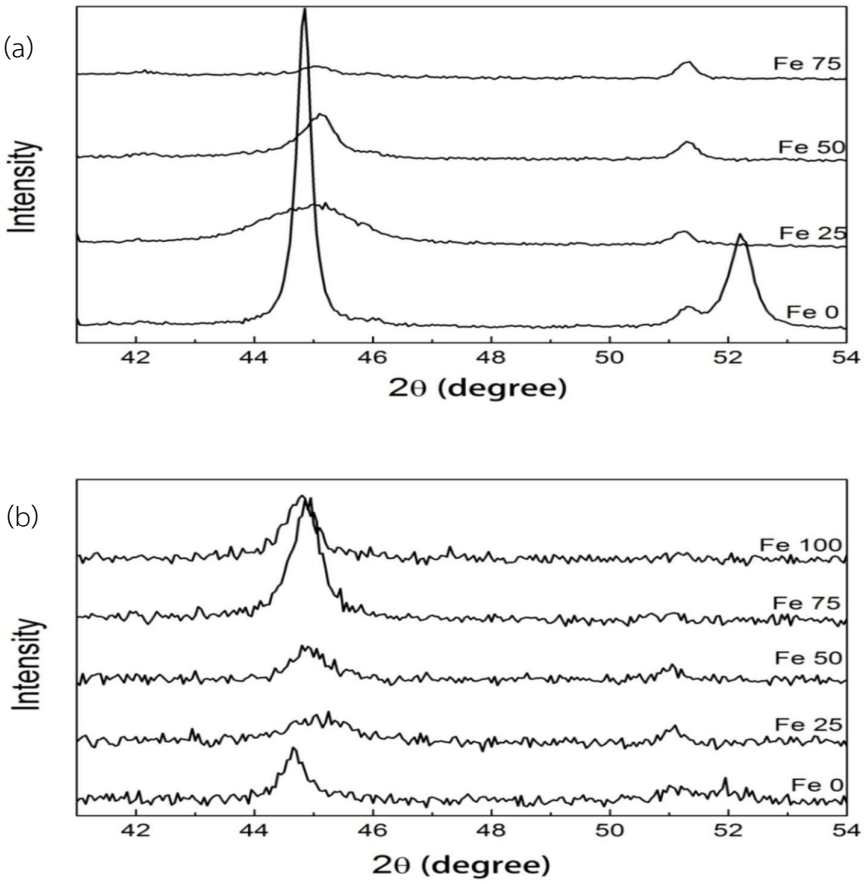

Figure 2.3 XRD patterns of Fe-Ni alloy thin films at various concentrations of iron ions of 100%, 75%, 50%, 25% and 0% (a) without saccharin and (b) with saccharin addition. X-ray diffraction peak profile is used for the determination of crystal structure, including d spacing and lattice constant. The results show the peak of BCC and FCC phases. Moreover,

the Fe-Ni alloy thin films are prepared by electrodeposition with varying the concentration of iron and nickel ions into 5 conditions. In addition, saccharin is used for additive in this electrolyte.

Moreover, the Fe-Ni alloy thin films were investigated structure by FCC (200) crystalline orientation around 51 to 52°. The XRD patterns show the diffraction peak at 51° in every ratio of iron ion and nickel ion. It can be implied that every ratios of the electrolyte with mixture of iron and nickel ion show the FCC structure when investigate by FCC (200) crystalline orientation. In addition, the XRD pattern of Fe 0 (Ni 100) shows 2 peaks around 51 to 52 ° of diffraction angel. When comparing this result with some literatures, it is found that the FCC from d_{200} can identify with 2 diffraction angle in different layer of film growth [9]. The decreasing of lattice constant is effected by increasing thickness of film. So, it can conclude that the nickel thin film that is prepared by electrodeposition shows the FCC structure in 2 thickness of thin film layer. However, the BCC phase can be investigated by the combination of FCC (111) and BCC (100) diffraction pattern at 2θ as 45°. So, it can be concluded that the structure of Fe-Ni alloy thin films are not homogenous in the entire alloy. The structure of film shows the cluster of FCC and BCC structure entire Fe-Ni thin film.

Furthermore, the XRD pattern of Fe-Ni alloy thin films at various concentrations of iron ions of 100%, 75%, 50%, 25% and 0% with saccharin addition is displayed in Figure 2.3 (b). The d_{110} BCC phase shows peak about $2\theta \approx$ 44-45 °. The other phase is FCC and the peaks of d_{111} and d_{200} shows at about $2\theta \approx$ 44-45 and $2\theta \approx$ 51. In addition, the formal crystal structure of iron is BCC and lattice constant is 2.87 Å. The lattice constant is calculated by the experiment in various concentrations of iron ions and nickel ions. In addition, at the Fe concentration of 100% and 75% show in Fig. 4.1(b). The XRD pattern exhibit only BCC phase because d_{200} pattern cannot be observed. The XRD patterns at Fe concentration of 50% and 25% showed both of FCC and BCC phase. The XRD of pure Ni film showed only FCC crystal structure because the 1st peak shows lower value of

diffraction angel. So, the XRD results of Fe-Ni alloy thin films can observe crystal structures of iron and nickel alloy and it changes from FCC to BCC at about 50 to 75 percentage of iron.

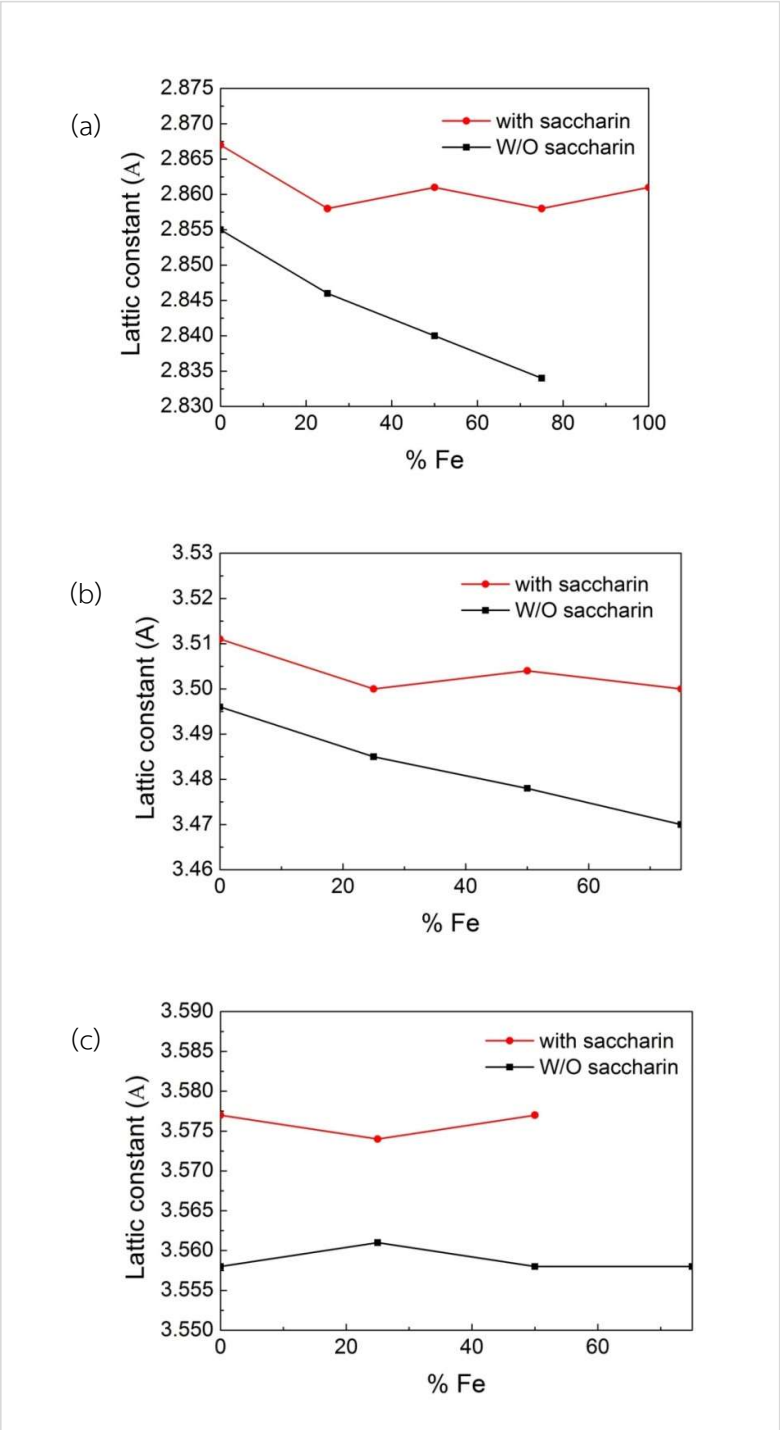

Figure 2.4 Lattice constant of Fe-Ni alloy thin films at various concentrations of iron ions with addition saccharin at (a) d_{110} BCC phase, (b) d_{111} and (c) d_{200} FCC phase.

Figure 2.4 (a), (b) and (c) shows the lattice constant of Fe-Ni alloy thin film at various concentrations of iron ions. It shows similarly trend that saccharin addition has an effect to the lattice constant. The Figure 2.4 shows increasing of lattice constant when adding saccharin. It can be implied that saccharin affects to crystal structure and crystallinity of alloy thin film. These results are also used for more discussion in next experiments.

For more structure investigation, the results are compared by with and without additive in the same composition of iron and nickel ion as shown in Fig. 2.5. The XRD patterns for ratio of iron ion and nickel ion as 75 to 25 are showed in Fig. 2.5(a). These results show the different peak of diffraction patterns. The d_{200} cannot observe with addition of saccharin that can de indicated the structure of Fe-Ni alloy thin film is BCC with addition of saccharin. However, d_{200} can be observed at 2θ as 51 ° that the electrolyte is not adding saccharin. This XRD diffraction angle shows the structure of FCC. So, it can be implied that addition of saccharin can affect the iron atoms deposit to be Fe-Ni alloy thin film more than without saccharin electrolyte. As saccharin content added, the BCC phase became the main phase, and the surface appearance became rough with faceted islands [10].

In addition, XRD patterns in another composition are showed in Figures 2.5 (b) and 2.5 (c). These patterns show the diffraction angle of addition saccharin similar to without saccharin although the addition saccharin XRD patterns show more noise than without saccharin. It can be implied that the saccharin has an effect to preparation of Fe-Ni alloy thin film. Iron can deposit to be thin film more than without saccharin addition. However, the electrolyte that without saccharin can deposit orderly thin films those are represent by the sharp peak and less noise with the same concentration of iron and nickel ion. In addition, the structures of Fe-Ni thin film are similar trend if the iron content in the electrolyte less than 75%.

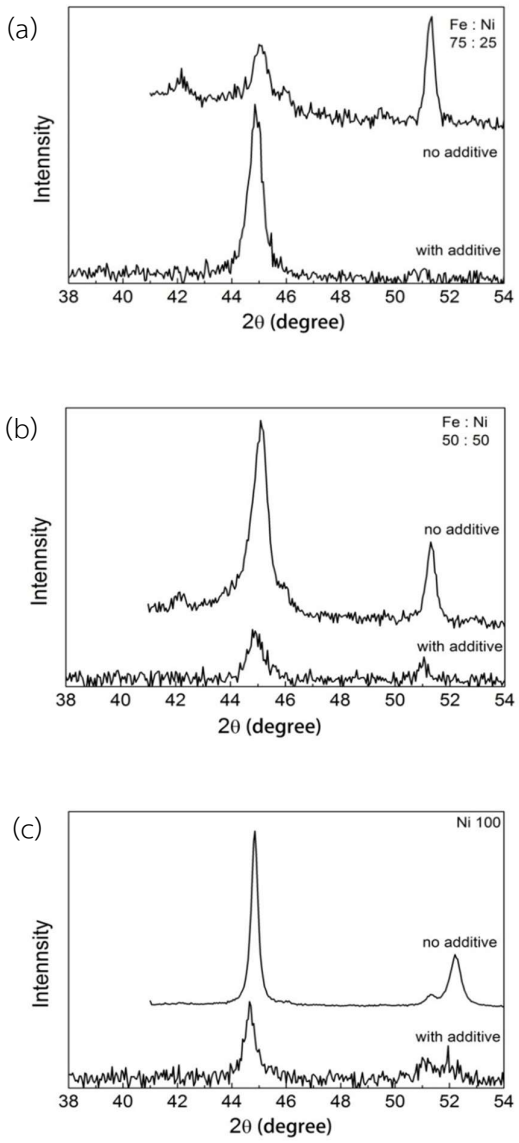

Figure 2.5 XRD patterns of Fe-Ni alloy thin films at various concentrations of iron ions of a) 75%, b) 50% and c) 0% with and without saccharin addition.

So, it can be concluded that the electrodeposited iron-nickel thin films are not atomically homogeneous. Thin films are not homogeneous in the entire alloy. At the low percentage of iron, the thin film must be FCC but we can observe the peaks of BCC. However, the intensity of FCC structure is more intense than BCC. It may cause of the few iron forming iron BCC structure or relocation nickel atoms in FCC. Both FCC and BCC can be founded in the alloy thin films. The structure converts from FCC to BCC when the composition of iron is about 35-50% with the addition of saccharin but the structures show the mixture phase of BCC and FCC when Fe-Ni alloy thin films are prepared by electrolyte that without saccharin. It can be indicated that saccharin affect to increase iron content in Fe-Ni thin films but the structure is similarly to without saccharin addition.

d. The effect of magnetic field on the formation of the Fe-Ni thin film

For studying the effect of magnetic field on the formation of the Fe-Ni thin film, the Fe-Ni alloy thin films are investigated by X-ray diffraction with adding the external magnetic field when thin films are prepared by electrodeposition. The external magnetic field is applied by hard magnet beside the electrodeposition bath in 3 sides including without magnetic field (No M), magnetic field at the anode (MA), cathode MC) and half side at anode (MA 50). The XRD patterns of applying external magnetic field during preparation are reported in Figures 2.6 (a), (b) and (c) in different concentration of iron and nickel ions in the electrolyte. These results show that the diffraction angle of every peak is the same trend with two high intensity peaks around 45° and 51°. The structure of those peaks is described by the previous results that show the external magnet field has not an effect to the structure of Fe-Ni alloy thin films. However, the relative of 1^{st} and 2^{nd} peaks are not similarly trend. The relative 1^{st} and 2^{nd} peak intensity are showed in Figure 2.7 These results show the effect of external magnetic field with the intensity of diffraction patterns. The increasing of relative depend on increasing of iron content in the electrolyte when compare with the

relative without magnetic field. It can be implied that the increasing of iron content has an effect to decrease the intensity of diffraction angle at FCC (200) crystalline orientation and the structure become to mixture BCC (110) and FCC (111) crystalline orientation. Moreover, the XRD patterns of applying the magnetic field at the cathode show the most value of relative at when comparing with another position of permanent magnet. It can be indicated that the FCC structure is apparently and BCC structure is reduced by applying magnetic field at the cathode. It may cause the magnet field oppose the initiation of iron films.

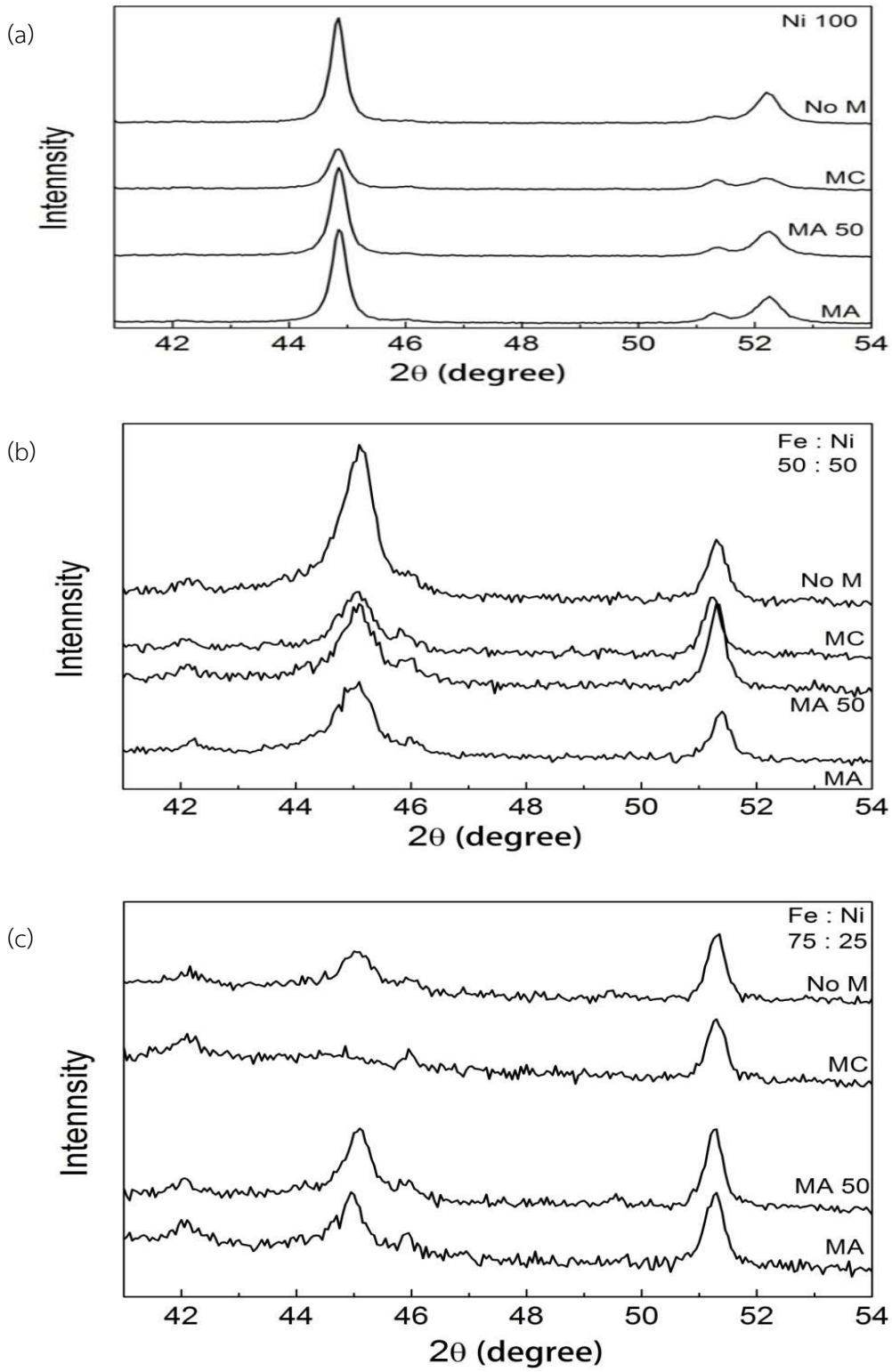

Figure 2.6 XRD patterns of Fe-Ni alloy thin films at various concentrations of iron ions of (a) 0%, (b) 50%, (c) 75% with 4 conditions of magnetic field.

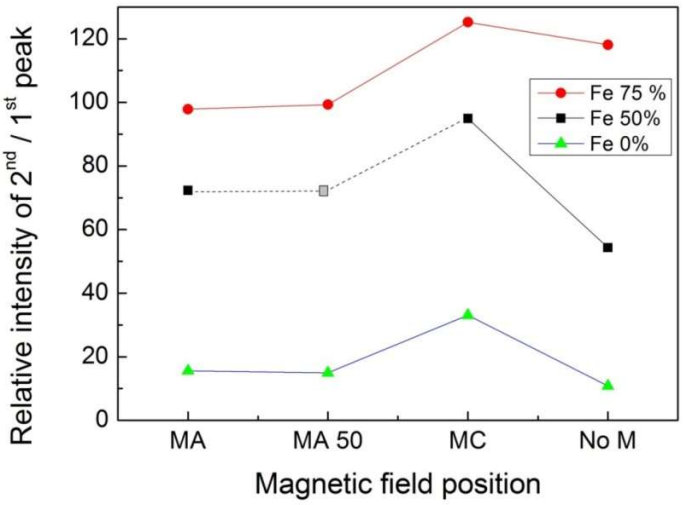

Figure 2.7 The relative XRD patterns of Fe-Ni alloy thin films at various concentrations of iron ions of (c) 75% and (d) The ratio of between the XRD intensities of the 2nd to the 1st peaks from Fe-Ni alloy thin films at various concentrations.

3. The development of magneto-optical Kerr effect measurement system

a. Introduction

In this research, the magneto-optical Kerr effect (MOKE) measurement system was developed to measure the magnetic properties of metal and organic thin films. The technique used in the set-up is beam on polarization modulation using a photo-elastic modulator (PEM). Two types of home-built magnets (copper-wire-coil electromagnet and movable permanent magnet) were also developed as a source of magnetic field. The MOKE measurement system was tested by measuring the magnetic properties of an electrodeposited Ni thin film.

b. The Set-up of the MOKE Measurement System

The instrumentation of the MOKE measurement is investigated in longitudinal and polar modes. The design and setup of the MOKE measurement are explained for optical setup and magnet design. The equipment for the MOKE measurement includes a laser, polarizers, a polarizing beam splitter (PBS), a photoelastic modulator (PEM), a detector, a lock-in amplifier, a digital multimeter, a d.c. power supply and an oscilloscope. The magnets used for the MOKE measurement were both home-made electromagnets (Figure 3.1) and a movable permanent magnet (Figure 3.2). The schematic diagram of L-MOKE and P-MOKE setups are shown in Figure 3.3 and 3.4, respectively. The setup of the polar mode is similar to that of the longitudinal mode except the orientation of applied magnetic field to sample. The orientation of the magnet can be changed between applying the magnetic parallel to the sample for the longitudinal mode and perpendicular to the film for the polar mode.

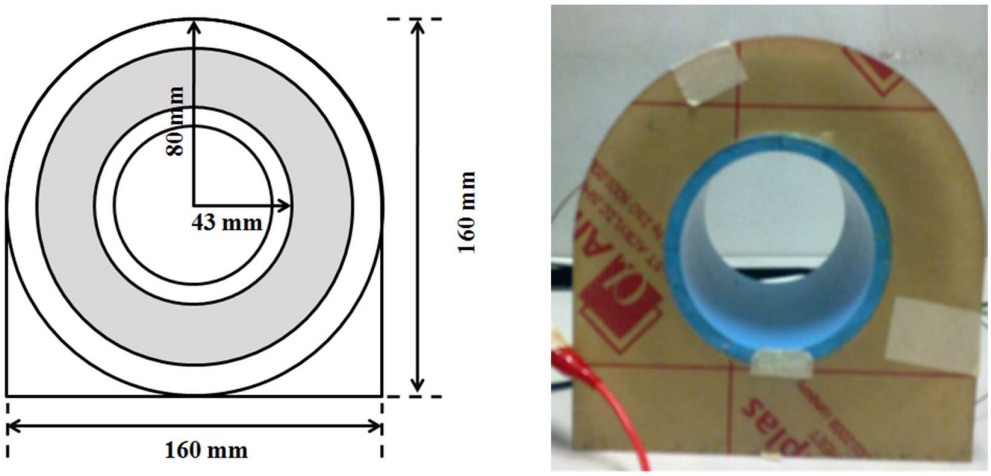

(a)

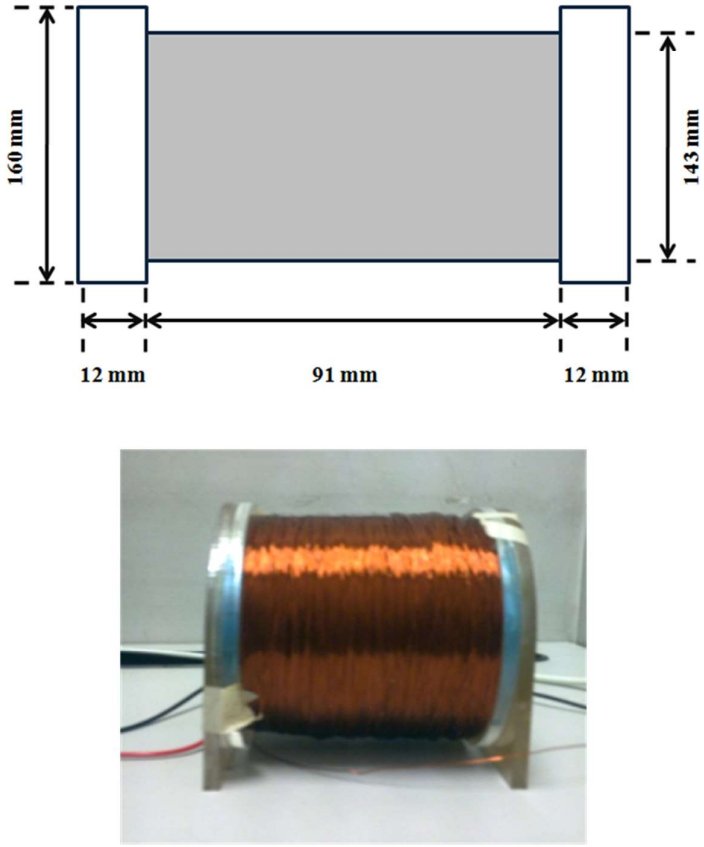

(b)

Figure 3.1 Design and construction of the home-made electromagnet; (a) front and (b) beside views.

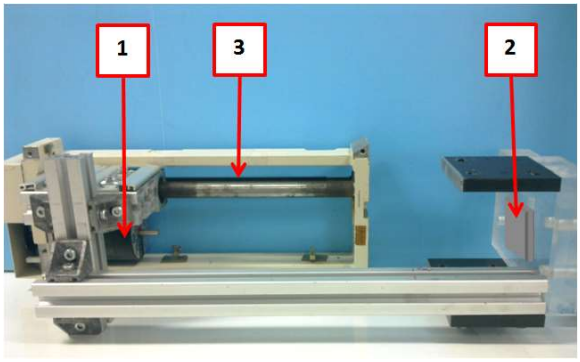

Figure 3.2 A movable permanent magnet, (1) stepping motor, (2) permanent magnet and (3) screw.

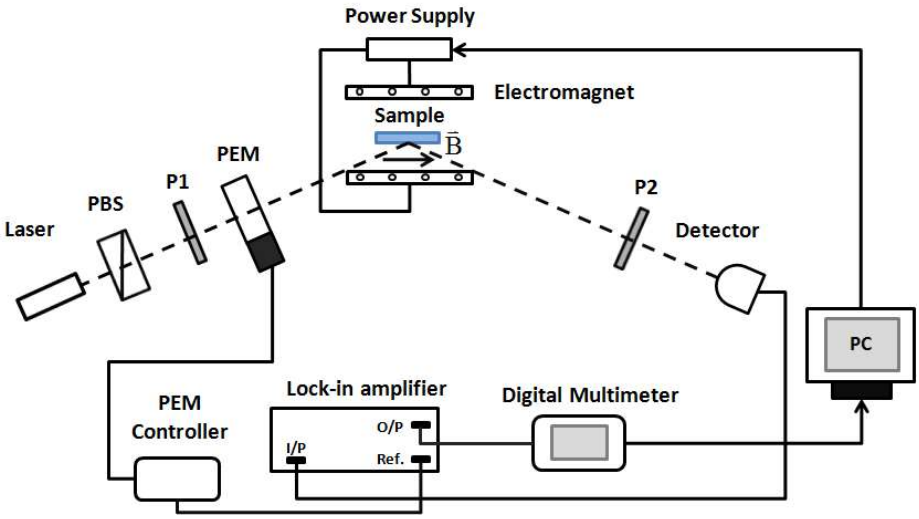

Figure 3.3 Schematic diagram for L-MOKE measurement setup.

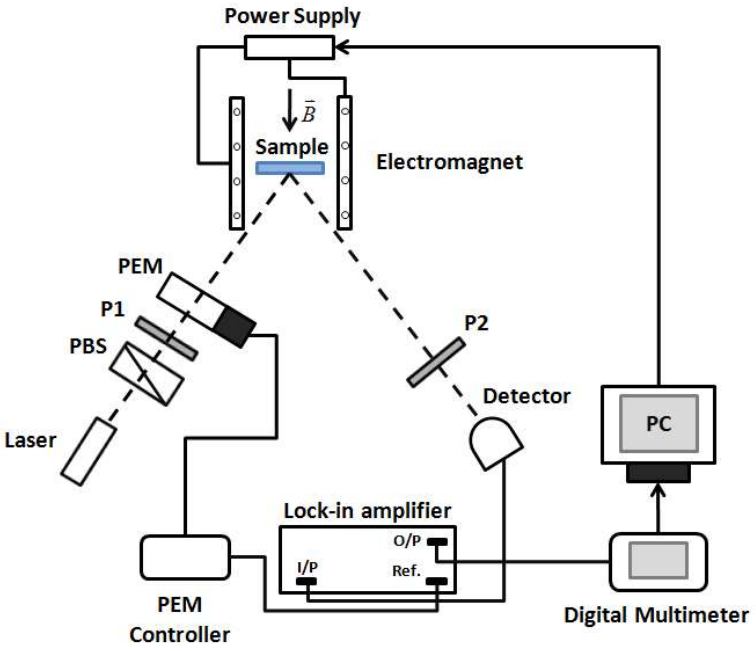

Figure 3.4 Schematic diagram for P-MOKE measurement setup.

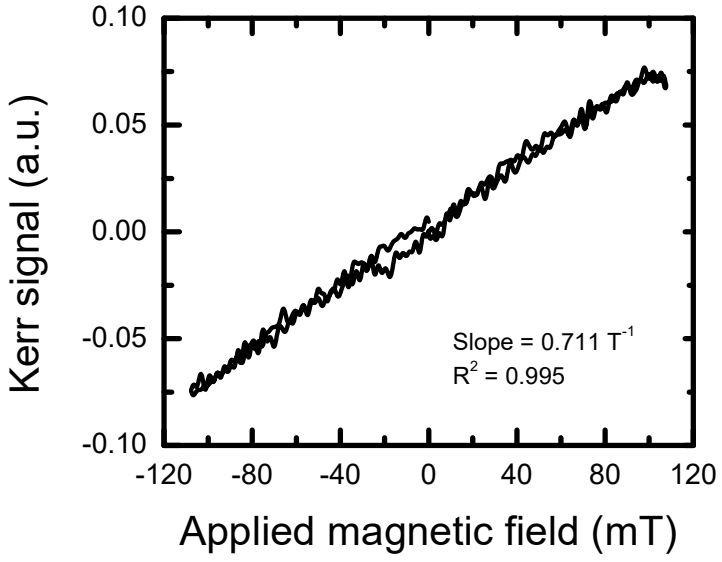

Figure 3.5 MOKE signal of electrodeposited Ni thin film (at first scan) using the home-made electromagnet.

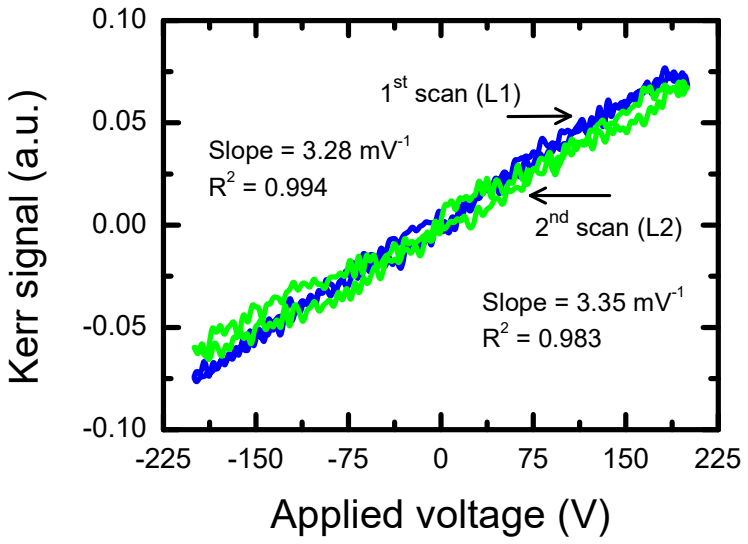

Figure 3.6 MOKE signal of electrodeposited Ni thin film (first and second scans) using the home-made electromagnet.

c. MOKE measurement for electrodeposited nickel thin films

The nickel films were prepared by electro-deposition technique. The sample with the size of 2.5×2.5 cm^2 was used to test the MOKE measurement.

The Longitudinal MOKE measurement (L-MOKE) signals of electrodeposited Ni thin film under applied magnetic field by both the movable permanent magnet and the home-made electromagnet are shown in Figure 3.5 and Figure 3.6, respectively. For both case, the L-MOKE signals increase linearly with the applied magnetic field.

The Polar MOKE measurement (P-MOKE) signals of electrodeposited Ni thin film under applied magnetic field by both the movable permanent magnet and the home-made electromagnet are shown in Figure 3.7 and Figure 3.8, respectively. For the measurement with the movable permanent magnet, the slope of the curve decreases gradually with the magnetic field indicating the tendency to be saturated of the magnetization of the film under the magnetic field. In this case, the saturated magnetization of electrodeposited Ni thin film can be observed with applied magnetic field near 65 mT. The coercive field of electrodeposited Ni thin film cannot be observed. These results are very noisy. It is

considered to be due to the vibration of the system from the movement of the permanent magnet during the measurement. For the measurement with the home-mad electromagnet, the saturated magnetization is observed with the applied magnetic field near 65 mT. The coercive field is observed with the applied magnetic field about 20 mT.

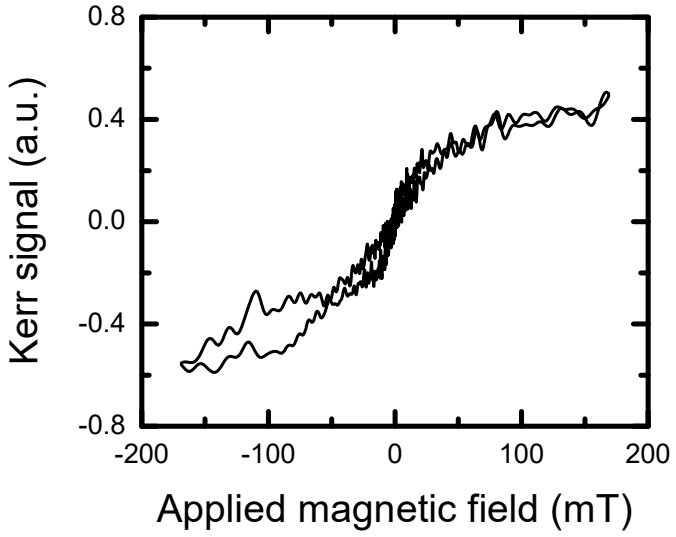

Figure 3.7 MOKE signal of electrodeposited Ni thin film measured in the polar mode using the moving permanent magnet.

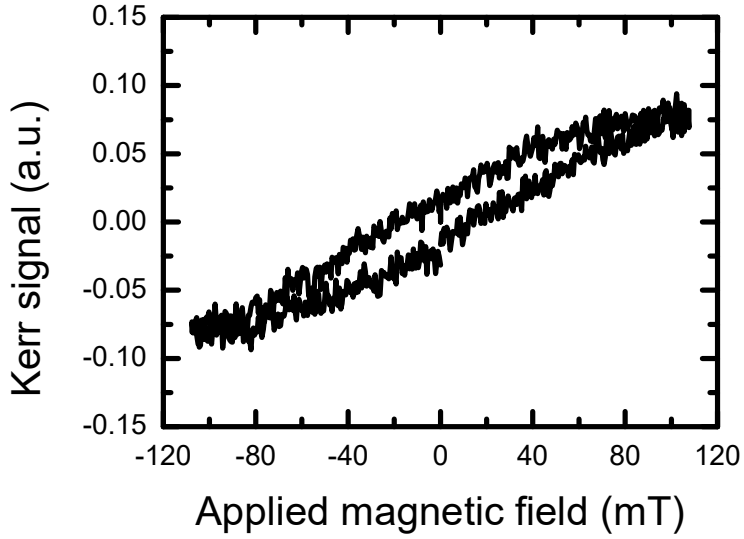

Figure 3.8 MOKE signal of electrodeposited Ni thin film for polar mode using the home-made electromagnet.

4. MOKE measurement of organic compounds

a. Introduction

In this research, the magneto-optical Kerr effect (MOKE) measurement system was used to study the magnetic properties of various kinds of metal-phthalocyanine thin films. The thin films were prepared by two techniques: and thermal evaporation and layer-by-layer (LBL) formation. The films prepared by the thermal evaporation are the film of metal-phthalocyanine (MPc) compounds, where as those prepared by the layer-by-layer formation are the film of metal tetrasulfonated phthalocyanines (MTsPcs). The molecular structures of some MPcs and MTsPcs are shown in Figure 4.1.

For the thermal evaporation, the MPcs were deposited on glass substrates by thermal evaporation. The pressure of the deposition reached 10^{-5} torr. The thickness of films was monitored in situ by a quartz-crystal oscillator. The deposition rate was controlled at 10 nm/min. In this thesis, the MPcs thin films such as FePc, CoPc and CuPc were used for the MOKE measurement. The film thickness of FePc, CoPc and CuPc thin films used in the the thesis are 90, 750, 100 nm, respectively.

For the layer-by-layer formation, the metal tetrasulfonated phthalocyanines (MTsPcs) such as FeTsPc, NiTsPc and CuTsPc molecules are used to prepare the layer-by-layer (LBL) organic thin film. The MTsPc molecules act as anionic polyelectrolyte since the substitution of peripheral ring with sulfonate groups in molecule can interact with cation of other compounds. The LBL multilayers of PAH/MTsPc thin films were prepared on glass substrates with MTsPcs and poly (allyamine hydrochloride) (PAH) solutions. The concentration of MTsPc and PAH solutions are 5×10^{-4} g/L in deionized water. The pH of MTsPc and PAH solutions were adjusted at to 7.5 and 3 by adding 0.1M of NaOH solution, respectively. The MTsPc act as polyanions whereas PAH acts as polycations. The glass substrate is immersed into aqueous PAH solution following by being rinsed in distilled water to remove un-adsorbed molecules. The glass is then immersed into aqueous MTsPc solution following by being

rinsed in distilled water. After this deposition cycle, the one bi-layer of PAH/MTsPc thin film is attached on the substrate. The process is repeated with a number of times to obtain the desired number of bi-layers. The MOKE measurements are performed with MTsPcs thin films such as FeTsPc, NiTsPc and CuTsPc. For FeTsPc and CuTsPc thin films, the numbers of bi-layers are 50 bi-layers. For NiTsPc thin film, the number of bi-layer is varied 5, 10, 20, 30, 40 and 50 bi-layers.

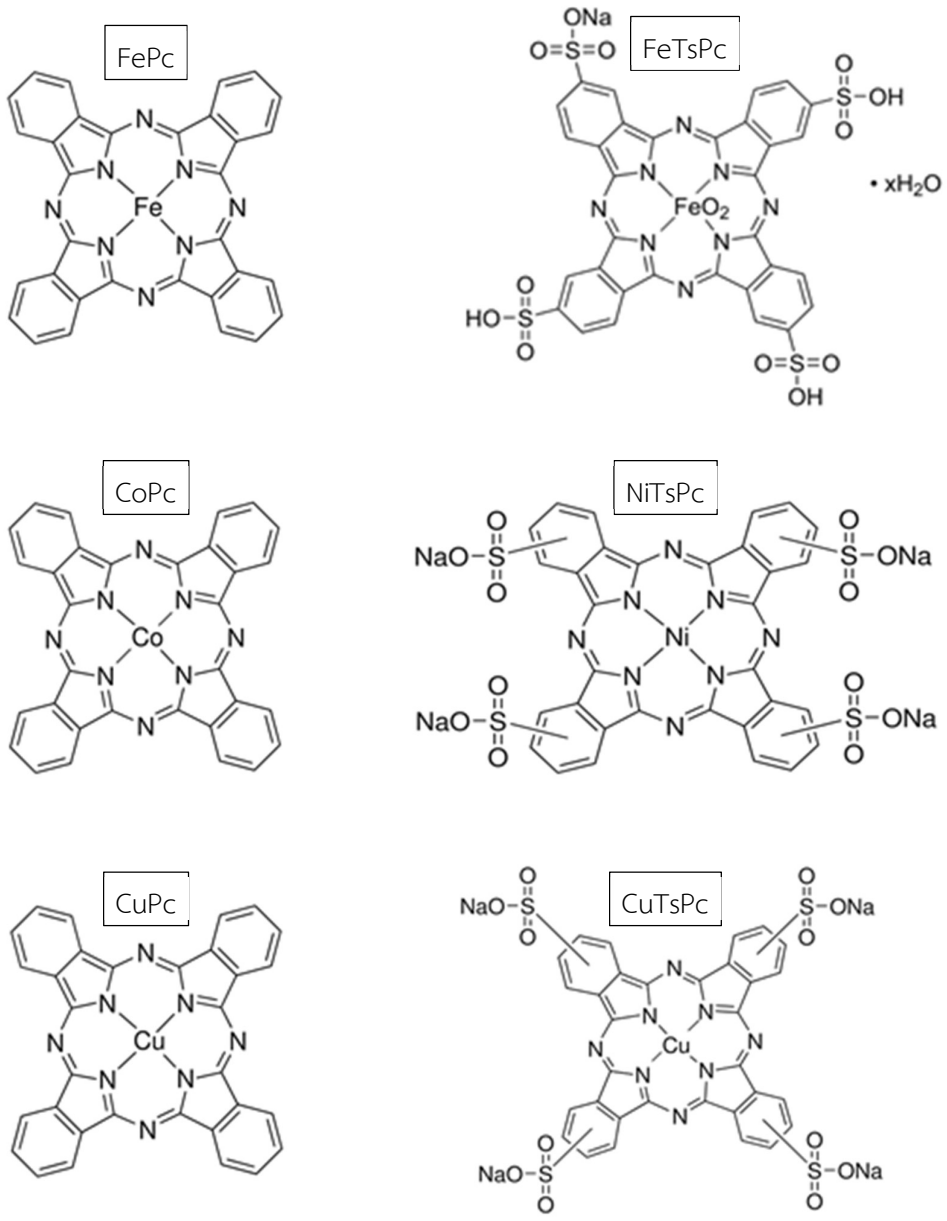

Figure 4.1 The molecular structures of some MPcs and MTsPcs

b. The MOKE measurements

The longitudinal MOKE of fabricated NiTsPc/PAH, FeTsPc/PAH and CuTsPc/PAH thin films were measured. The slope of the MOKE signal can be related to the magnetic susceptibility of the sample. For NiTsPc/PAH LbL thin film, the number of bi-layer was varied from 5 to 50 bi-layers. The MOKE signal of NiTsPc/PAH thin film can be observed, with non-

zero slope, for only the numbers of bi-layers of 10, 30 and 50 as shown in Figures 4.2 and 4.3. The MOKE signal can be detected pronouncedly for the case of the films with more than 30 bi-layers. When the number of bi-layers increases from 40 to 50 bi-layers, the slopes of the MOKE signal do not change significantly. This is due to the interaction between the light and the material occurs only at the film surface for the reflection configuration.

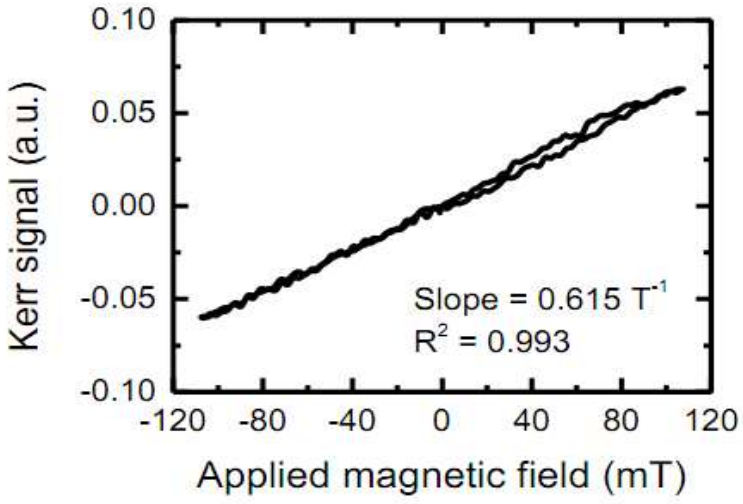

Figure 4.2 MOKE measurement of NiTsPc/PAH thin films for 50 bilayers.

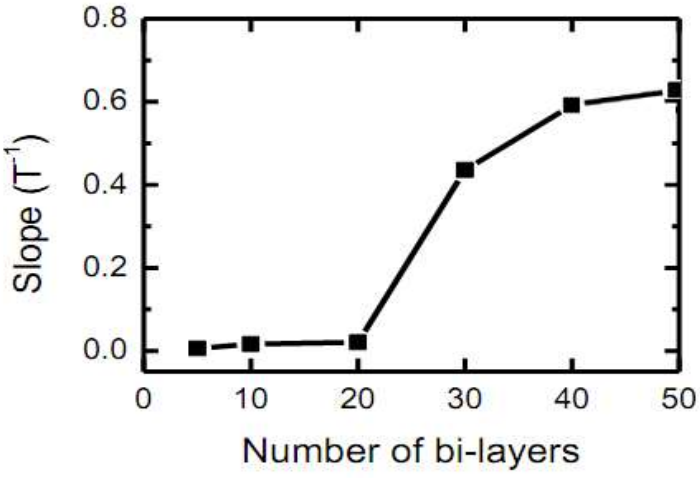

Figure 4.3 The slope of MOKE signal from NiTsPc as a function of numbers of bilayers.

The evaporated MPc thin films are also used to measure the longitudinal MOKE. As shown in Figure 4.4, the MOKE signal for evaporated CoPc thin film exhibits the almost linear line as a function of applied magnetic field with the MOKE signal slope of 5.72 1 T^{-1}. This slope value is very much higher than the slope value of 0.615 T^{-1} for NiTsPc/PAH nanostructure. This result corresponds to the strengthening of magnetization for CoPc and NiPc molecules.

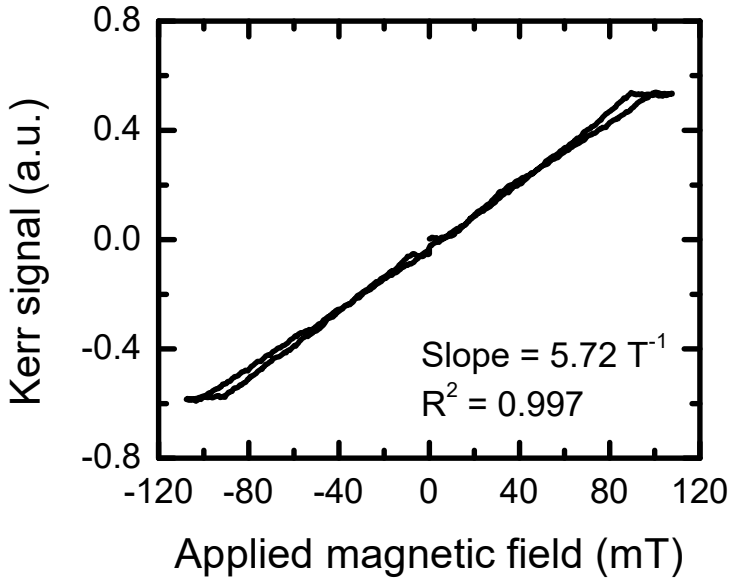

Figure 4.4 MOKE signal of evaporated CoPc thin film

The MOKE signals of nanostructures for FeTsPc/PAH and evaporated FePc thin film are measured and compared in Figure 4.5 since both structures have Fe ion at the center of the molecule. The FeTsPc/PAH LbL thin films consists of 50 bilayers. The MOKE signal of both FeTsPc/PAH and FePc thin films increases linearly with applied magnetic field. The MOKE signal of FeTsPc/PAH thin film is much stronger than that of NiTsPc/PAH thin films. It can be noticed that the slopes of MOKE signal of evaporated FePc and LbL structure of FeTsPc/PAH have about the same values of 3.21 and 3.28 T^{-1}, respectively. This can be confirmed that the MOKE signal does not depend on neither the fabrication technique nor the organic chemical formula since Kerr effect mainly occurs between the metal atom.

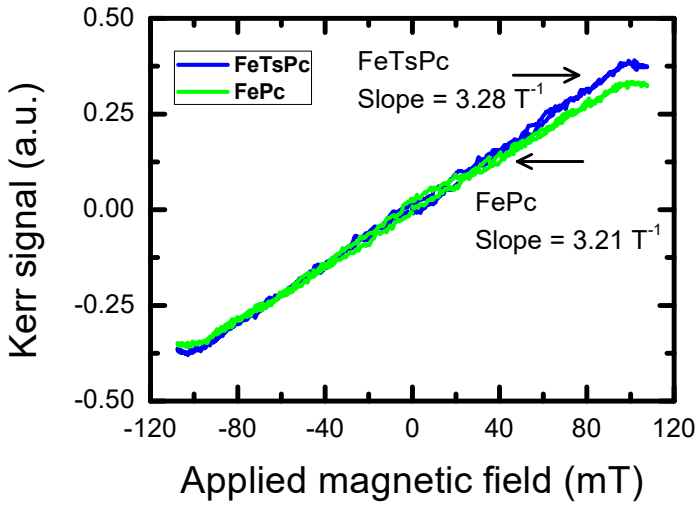

Figure 4.5 MOKE signal of evaporated FePc thin film and 50 bi-layers of FeTsPs/PAH

In addition, the MOKE signals of evaporated CuPc thin film and 50 bilayers of CuTsPc/PAH nanostructure are also investigated and compared as illustrated in Figure 4.6. The MOKE signal of CuTsPc/PAH is slightly greater than that of NiTsPc/PAH thin film. While the MOKE signal of CuPc is the weakest among evaporated thin flims. Moreover the slopes of MOKE signal for CuPc and CuTsPs structures have about the same values of 0.849 and 0.713 T^{-1}, respectively. This also demonstrates independence of fabrication techniques and different in organic molecules.

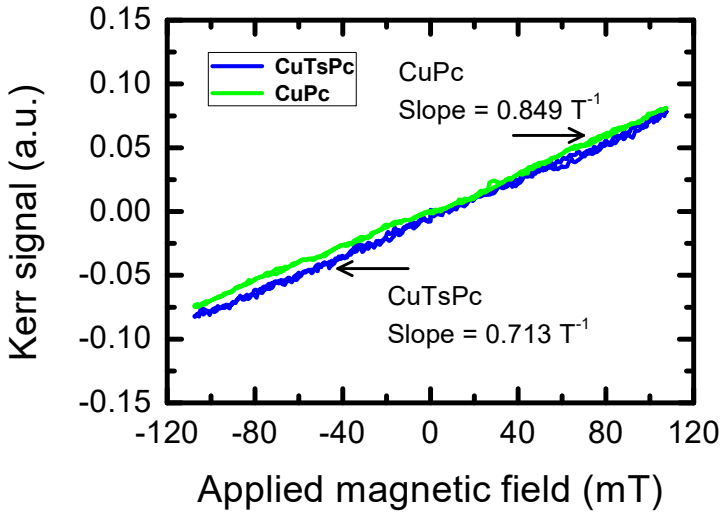

Figure 4.6 MOKE signal of evaporated CuPc thin film and 50 bilayers of CuTsPs.

Slope of the MOKE signal can be related to the magnetic susceptibility of the sample. The slope of MOKE signals for FeTsPc/PAH, CuTsPc/PAH and NiTsPc/PAH thin films with 50 bi-layers are 3.28, 0.713 and 0.615 T^{-1}, respectively. While the values for evaporated FePc, CuPc and CoPc thin films are 3.21, 0.849 and 5.72 T^{-1}, respectively. The slope of MOKE signal which can relate to the magnetic strength are plotted as a function of metal atom at the center of MPc molecule as demonstrated in Figure 4.7. In addition, the calculated magnetic moment of FePc, CuPc and NiPc molecules are 2.54, 1.61 and 0.14 μ_B, respectively [11], [12]. The trend of these calculated results is qualitatively similar to the trend of the strength of the MOKE signals from the experiment. The experimental values of the results of sample with the same kind of metal atom but prepared different techniques are very close and considered to be approximately the same value. Actually the ZnPc thin film is also fabricated by thermal evaporation and conduct the MOKE measurement. However with our sensitivity, it cannot be observed the Kerr effect and reported its slope as a zero in the graph.

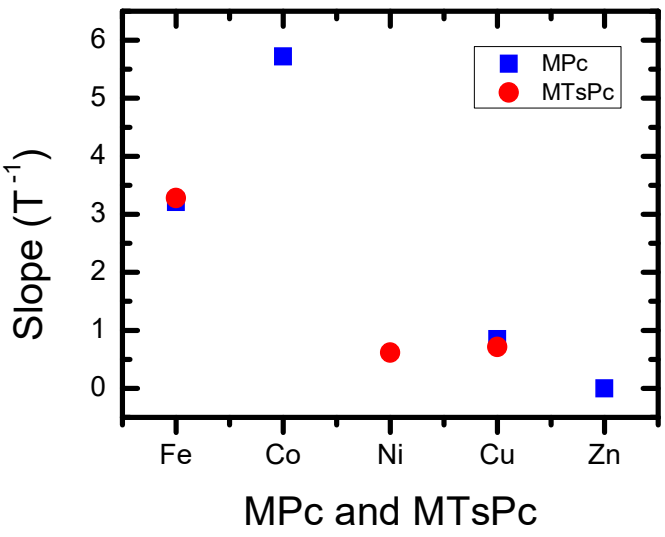

Figure 4.7 Slopes of MOKE signals for various metal atom in MTsPc LbL thin films and evaporated MPc thin films

From the measurement, the magnetic susceptibility of FePc or FeTsPc structures can be estimated to be strongest among the invesitigated MPc and MTsPc structures. By comparing the slope of MOKE signal of our MOKE measurement at room temperature and the calculated magnetic moment at 0 K, the tendency of the slope of MOKE signal of the MOKE measurement is similar to those of the magnetic moments of various MPc molecules.

Reference

[1] W. J. M. Naber, S. Faez, and W. G. van der Wiel, “Organic spintronics,” *J. Phys. Appl. Phys.*, vol. 40, no. 12, pp. R205–R228, Jun. 2007, doi: 10.1088/0022-3727/40/12/R01.

[2] Y. Zhan and M. Fahlman, “The study of organic semiconductor/ferromagnet interfaces in organic spintronics: A short review of recent progress,” *J. Polym. Sci. Part B Polym. Phys.*, vol. 50, no. 21, pp. 1453–1462, 2012, doi: 10.1002/polb.23157.

[3] K. Ando, “Magneto-optical studies of s,p–d exchange interactions in GaN:Mn with room-temperature ferromagnetism,” *Appl. Phys. Lett.*, vol. 82, no. 1, pp. 100–102, Jan. 2003, doi: 10.1063/1.1534618.

[4] S.-H. Kim *et al.*, “Effect of saccharin addition on the microstructure of electrodeposited Fe–36 wt.% Ni alloy,” *Surf. Coat. Technol.*, vol. 199, no. 1, pp. 43–48, Sep. 2005, doi: 10.1016/j.surfcoat.2004.11.035.

[5] J. Yu, M. Wang, Q. Li, J. Yang, and L. Liu, “Effects of saccharin on microstructure and property of electro-deposited Ni-Fe alloys,” *Trans. Nonferrous Met. Soc. China*, vol. 19, no. 4, pp. 805–809, Aug. 2009, doi: 10.1016/S1003-6326(08)60354-4.

[6] V. C. Kieling, “Parameters influencing the electrodeposition of Ni-Fe alloys,” *Surf. Coat. Technol.*, vol. 96, no. 2, pp. 135–139, Nov. 1997, doi: 10.1016/S0257-8972(97)00078-9.

[7] C. Su, F. He, H. Ju, Y. Zhang, and E. Wang, “Electrodeposition of Ni, Fe and Ni–Fe alloys on a 316 stainless steel surface in a fluorborate bath,” *Electrochimica Acta*, vol. 54, no. 26, pp. 6257–6263, Nov. 2009, doi: 10.1016/j.electacta.2009.05.076.

[8] T. Otiti, G. I. Ekosse, and T. S. Sathiaraj, “Understanding Nickel Thin Film crystallization using X-Ray Diffractometry,” *J. Appl. Sci. Environ. Manag.*, vol. 11, no. 2, Art. no. 2, 2007, doi: 10.4314/jasem.v11i2.54986.

[9] D. E. Sayers, E. A. Stern, and F. W. Lytle, “New Technique for Investigating Noncrystalline Structures: Fourier Analysis of the Extended X-Ray---Absorption Fine Structure,” *Phys. Rev. Lett.*, vol. 27, no. 18, pp. 1204–1207, Nov. 1971, doi: 10.1103/PhysRevLett.27.1204.

[10] H. D. Arnold and G. W. Elmen, “Permalloy, A New Magnetic Material of Very High Permeability,” *Bell Syst. Tech. J.*, vol. 2, no. 3, pp. 101–111, 1923, doi: 10.1002/j.1538-7305.1923.tb03595.x.

[11] X. Shen *et al.*, “Spin transport properties of 3d transition metal(II) phthalocyanines in contact with single-walled carbon nanotube electrodes,” *Phys. Chem. Chem. Phys.*, vol. 12, no. 36, pp. 10805–10811, Sep. 2010, doi: 10.1039/C002301A.

[12] P. Gargiani *et al.*, “Spin and orbital configuration of metal phthalocyanine chains assembled on the Au(110) surface,” *Phys. Rev. B*, vol. 87, no. 16, p. 165407, Apr. 2013, doi: 10.1103/PhysRevB.87.165407.

5. Outputs from the Research Projects

a. Published Articles in International Journals

(1) W. Limphirat, W. Inprasit, T. Juagwon, P. Prachopchok, M. Duriyarattakarn, **A. Sinsarp**, K. Tivakornsasithorn, and T. Osotchan, “In-situ monitoring of electro-deposition for iron-nickle thin film by time-resolved X-ray absorption spectroscopy”, Materials Today: Proceedings 5, 10997 (2018).

(2) Ketwadee Wetsuwan, Prathan Prachopchok, Theerasak Juagwon, Wanwisa Limphirat, Kritsanu Tivakornsasithorn, **Asawin Sinsarp**, Tanakorn Osotchan, "Thermal annealing effect on real time atomic relocation of iron-cobalt alloys prepared by electro-deposition", Advanced Materials Research 1103, 69 (2015)

(3) Teerapat Rutirawut, Wanwisa Limphirat, **Asawin Sinsarp**, Kritsanu Tivakornsasithorn, Toemsak Srikhirin and Tanakorn Osotchan , “Composition and Oxidation State of Cobalt- and Nickel-Iron Oxide Colloidal Nanoparticles in Liquid Phase”, Advanced Materials Research 1103, 69 (2015)

(4) Y. Yokoyama, **Asawin Sinsarp**, Y. Yamada, H. Asaoka and M. Sasaki, "Ordering of C60 on one-dimensional template of single-domain Ge(110)-16×2 and Si(110)-16×2 surfaces”, Applied Physics Express, 5, 025203 (2012)

(5) Y. Yokoyama, H. Asaoka, **Asawin Sinsarp** and M. Sasaki, “One-dimensional nanotemplate structure of a Si(110) substrate”, e-Journal of Surface Science and Nanotechnology, 10, 509 (2012)

b. Internation conference proceeding

(1) Teerapat Rutirawut, **Asawin Sinsarp**, Kritsanu Tivakornsasithorn, Toemsak Srikhirin, Tanakorn Osotchan,"Phase shift on reflection from polystyrene colloidal photonic crystal film on hydrogel surface”, Proceedings of SPIE - The International Society for Optical Engineering, 9659, 96590I, (2nd International Conference on Photonics Solutions, Hua Hin, Thailand, 6 - 8 July 2015 through 8 July 2015)

c. National Conference Proceedings

(1) P. Srisawet, **Asawin Sinsarp**, K. Tivakornsasithorn, and T. Osotchan, “Developing of Magneto–Optical Kerr Effect Measurement Setup by using a home–made

Electromagnet and a moving Permanent Magnet for Investigating the Magnetic Properties of Nickel and Metal–Phthalocyanine Films", SPC2013

(2) T. Rutirawut, **Asawin Sinsarp**, K. Tivakornsasithorn, T. Srikhirin, T. Osotchan, "Effect of Surfactant on Prepared Polystyrene-Iron Oxide Composite Nanoparticles", SPC2013

d. International Conference Presentations

(1) Teerapat Rutirawut, Wanwisa Limphirat, **Asawin Sinsarp**, Kritsanu Tivakornsasithorn, Toemsak Srikhirin and Tanakorn Osotchan , "Composition and Oxidation State of Cobalt- and Nickel-Iron Oxide Colloidal Nanoparticles in Liquid Phase", The 4th German-Thai Symposium on Nanoscience and Nanotecnology, October 14-17, 2014, Phitsanulok, Thailand

(2) Ketwadee Wetsuwan, Prathan Prachopchok, Theerasak Juagwon, Wanwisa Limphirat, Kritsanu Tivakornsasithorn, **Asawin Sinsarp**, Tanakorn Osotchan, "Thermal annealing effect on real time atomic relocation of iron-cobalt alloys prepared by electro-deposition", The 4th German-Thai Symposium on Nanoscience and Nanotecnology, October 14-17, 2014, Phitsanulok, Thailand

(3) Patawee Srisawet, **Asawin Sinsarp**, Kritsanu Tivakornsasithorn and Tanakorn Osotchan, "Magneto-Optical Kerr Effect of Various Metal Phthalocyanine Nanostructures prepared by different Techniques", The 4th German-Thai Symposium on Nanoscience and Nanotecnology, October 14-17, 2014, Phitsanulok, Thailand

(4) A. Thangprasert, P. Pasitsupparoad, **Asawin Sinsarp** and T. Osotchan, "Electrochemical Investigation of Phthalocyanine Layer-by-Layer (LbL) Thin Films Incorporating Carbon Nanotubes", NanoThailand 2012, April 9 - 12, 2012 , Khon Kaen, Thailand

(5) Ketwadee Wetsuwan, Rawat Jaisutti, Manus Sittishoktram, **Asawin Sinsarp**, Tanakorn Osotchan, Effect of Polyvinyl Acetate Mixture on Surface Morphology of Iron Oxide Thin Films Prepared by Spin Coating of Aluminium Ferric Oxalate, NanoThailand 2010, 18 November 2010, Bangkok, Thailand

e. National Conference Presentations

(1) Teerapat Rutirawut, Wanwisa Limphirat, **Asawin Sinsarp**, Kritsanu Tivakornsasithorn and Tanakorn Osotchan, "Determination of Iron Oxidation State in Iron Oxide, Cobalt- and Nickel-Ferrite Colloidal Nanoparticles by XANES", SPC2014, Nakornratchsrima, March 26-28, 2014

(2) W.Inprasit, M. Duriyarattakarn, **Asawin Sinsarp** and T. Osotchan, "Calculated Result Comparison of X-ray Absorption Spectroscopy of Fe-Ni Metal Alloy with Different Crystal Structure", SPC2014, Nakornratchsrima, March 26-28, 2014

(3) Ketwadee Wetsuwan, Wanwisa Limphirat, **Asawin Sinsarp**, Kritsanu Tivakornsasithorn, and Tanakorn Osotchan, "Magnetic Properties of Iron Oxide Thin Films Prepared from Annealed Electrodeposite Metal Films", SPC2014, Nakornratchsrima, March 26-28, 2014

(4) Patawee Srisawet, Aussadaporn Thangprasert, **Asawin Sinsarp**, Kritsanu Tivakornsasithorn, and Tanakorn Osotchan, "Magneto-Optical Kerr Effect Measurement of Various Metal hthalocyanine Thin Films Prepared by Layer by Layer Technique", SPC2014, Nakornratchsrima, March 26-28, 2014

(5) K. Wetsuwan, **Asawin Sinsarp**, T. Rutirawut, K. Tivakornsasithorn and T. Osotchan, "Preparation and Magnetic Properties of Iron Oxide/Organic Conductor Multilayered Thin Films by Spin Coating Technique", SPC2013

(6) Patawee Srisawet, Rawat Jaisutti, **Asawin Sinsarp**, Tanakorn Osotchan , "OPTICAL PROPERTIES TOGETHER WITH THEIR POLARIZATION AND MAGNETIC-FILED EFFECTS OF ZINC PHTHALOCYANINE THIN FILMS EXPOSED TO ACETONE," 37th Congress on Science and Technology of Thailand, October 10 –12, 2011, Bangkok, Thailand.

(7) Ketwadee Wetsuwan, **Asawin Sinsarp**, Atsadaporn Thangprasert, Tanakorn Osotchan, "ELECTRICAL PROPERTIES OF NICKEL TETRASUFONATED PHTHALOCYANINE – POLY(ALLYLAMINE HYDROCHLORIDE) MULTIBILAYER THIN FILMS," 37th Congress on Science and Technology of Thailand, October 10 –12, 2011, Bangkok, Thailand.

(8) Ketwadee Wetsuwan, **Asawin Sinsarp**, Rawat Jaisutti, Teerapat Rutirawut and Tanakorn Osotchan "Preparation and Properties of Iron Oxide Thin Films on Indium-Tin-Oxide-Coated-Glass Substrates by Spin Coating of Ammonium Ferric

Oxalate Solution", Siam Physics Congress 2011, Pattaya, Chonburi, THAILAND, March 23, 2011.

(9) Pattawee Srisawet, Rawat Jaisutti, **Asawin Sinsarp**, and Tanakorn Osotchan "Optical Polarization Effect of Treated Zinc Phthalocyanine Thin Films", Siam Physics Congress 2011, Pattaya, Chonburi, THAILAND, March 23, 2011.

(10) Teerapat Rutirawut, **Asawin Sinsarp**, and Tanakorn Osotchan "Calculation of Force Acting on Magnetically Controllable Colloidal Nanoparticles with Various Distributions", Siam Physics Congress 2011, Pattaya, Chonburi, THAILAND, March 23, 2011.

(11) **Asawin Sinsarp**, Manas Sittishoktram, Rawat Jaisutti, Tanakorn Osotchan, "Preparation of Iron Oxide/Poly(3-hexylthiophene) Bilayer Thin Films by Spin Coating Technique, The 36th Congress on Science and Technology of Thailand, 27 October 2010, Bangkok

(12) Patawee Srisawet, **Asawin Sinsarp**, Rawat Jaisutti, Tanakorn Osotchan, Study of Optical Properties and Their Polarization Effect of Copper-Phthalocyanine Thin Films, The 36th Congress on Science and Technology of Thailand, 27 October 2010, Bangkok

ภาคผนวก

Available online at www.sciencedirect.com

ScienceDirect

Materials Today: Proceedings 5 (2018) 10997–11003

materialstoday: PROCEEDINGS

www.materialstoday.com/proceedings

NanoThailand2016

In-situ monitoring of electro-deposition for iron-nickle thin film by time-resolved X-ray absorption spectroscopy

Wanwisa Limphirat[a,*], W. Inprasit[b], T. Juagwon[b], P. Prachopchok[b], M. Duriyarattakarn[b], A. Sinsarb, K. Tivakornsasithorn[b], and T. Osotchan[b]

[a]*Synchrotron Light Reasearch Institute, PO. Box 93, Nakhon Ratchasima 30000 THAILAND*
[b]*Materials Science and Engineering program, Capabi lity Building Unit of Nanosciences and Nanotechnology, Faculty of Science, Mahidol University,Bangkok, 10400 Thailand*

Abstract

The crystal structure of iron-nickel thin films depends on the composition of iron and nickel dissolved with electrolytes. However, it is believed that in electro-deposition the iron and nickel ions are homogenous distribute in the solution and should provide the uniformly homogenous alloy thin film. Due to differences in ion mobility and sticking condition of iron and nickel ions, the real time investigation of electro-deposition of these alloy thin films were investigated by TRXAS during the applying current into the solution. In this work, the electrochemical cell consists of two 2.0 x 2.0 cm^2 indium tin oxide (ITO) coated on thin plastic sheets for anode and cathode. These two electrodes separate by placing other two thin plastic sheets at the edges with the total thickness of 0.1 cm. The electrochemical cell is electro-deposited at the current density value of 0.25 mA/cm-2 for 10 minutes and collect the TRXAS data every 20 s with Fe *K*-edge (7112 eV) and Ni *K*-edge (8333 eV) at beam line 2.2, Synchrotron Light Research Institute (SLRI). Moreover, the intensity of X-ray at Fe edge dramatically decreases as the Fe ion deposits on the electrode. The slightly shift of Fe edge indicate the metal film forming i.e. Fe(II) ions convert to Fe(0) film. In addition, the signal of Fe(II) ion in R space also decrease as increasing the deposition time while the component at the nearest neighbor position of Fe metal alloy (at about 2Å) slight increase. However, the scattering signal of alloy at 1st nearest neighbor cannot determine the BCC and FCC crystal structure. These are needed the signal at the third and fourth nearest neighbor which are very weak at this initial deposition.

Selection and/or Peer-review under responsibility of The 5th Thailand International Nanotechnology Conference (NanoThailand2016).

Keywords: In-situ monitoring, Electrodepositon, Time-resolved X-ray absorption spectroscopy, Fe-Ni alloys ;

* Corresponding author. Tel.: +66-44-217040 ext 1480; fax: +66-44-217047.
E-mail address: wanwisa@slri.or.th

Selection and/or Peer-review under responsibility of The 5th Thailand International Nanotechnology Conference (NanoThailand2016).

1. Introduction

The Fe_xNi_{1-x} alloy thin films have been prepared by different techniques, such as mechanical alloying, sputtering, organic gel-thermal reduction process and electro-deposition. However, the electro-deposited technique allows the mass production that can control the compositions of alloy thin films and low cost comparing to other techniques.

Moreover, many researchers were studied local structure of Fe_xNi_{1-x} alloy thin film by XAS [4-6]. They used this technique to describe crystal structure. The crystal structure of iron is base center cubic (BCC) which nickel crystal is face center cubic (FCC). The distance of nearest neighbor atom was determined by this technique [7]. In addition, we observed the distance of nearest neighbor atom slightly changed when the structure of FexNi1-x alloy thin film convert from BCC to FCC.

In this study, we monitor the deposition of Fe_xNi_{1-x} alloy thin films by measuring x-rays absorption of the electrochemical cell during the electro-deposition process. The electrochemical cell consists of two thin plastic sheets coated by indium tin oxide (ITO) for anode and cathode electrodes. During electro-deposition for 10 minutes, the time-resolved x-ray absorption spectroscopy (TRXAS) was collected every 20 second at beam line 2.2, Synchrotron Light Research Institute (SLRI). The TRXAS at beam line 2.2 can collect data with the fastest readout speed of 25 ms [8]. The short data collection time opens an opportunity for TRXAS experiments such as studies of changes of the electronic structures or the local structure of an atom during a change in electro-deposition cell.

2. Illustrations

The Fe_xNi_{1-x} metal alloy thin films were prepared by electro-deposited on 2.0 x 2.0 cm^2 indium tin oxides (ITO) coated thin plastic sheets. The ITO coated thin plastic sheets were used for both anode and cathode electrodes and were parallel placed separately by other two thin plastic sheets with the U shape at the total thickness of 1.0 mm, as shown in Fig. 1. In addition in some experiments, the ITO coated thin plastic was patterned to be thin straight line with the line width of 2.0 mm in order to control the depositing area of Fe-Ni alloy thin film to become about at the position of the x-rays beam.

The $Ni(II)SO_4$ and $Fe(II)SO_4$ solutions were used as the sources of Ni and Fe ions and the compositions of Fe and Ni ions in electrolyte were modified by varying the ratio of $Ni(II)SO_4$ and $Fe(II)SO_4$ solutions including 100:0, 85:15, 75:25, 65:35 50:50, 35:65, 25:75, 15:85 and 0:100. The chemical compounds are dissolved with ultra-high purity de-ionized water. Boric acid, Na2SO4 and saccharin were added to the solutions and the pH of the solution was adjusted to be 2.0 by 1 M HCl. In addition, the current density value of 0.25 mA/cm^2 was used for the electro-deposition for 10 minutes. This electro-chemical cell was sufficient thin and light to allow some x-rays can pass through then the x-rays absorption (XAS) spectra can be collected every 20 second around Fe K-edge (7112 eV) and Ni K-edge (8333 eV) at beam line 2.2, Synchrotron Light Research Institute. The experimental data were averaged and normalized using Demeter package version 0.9.18.2 [9].

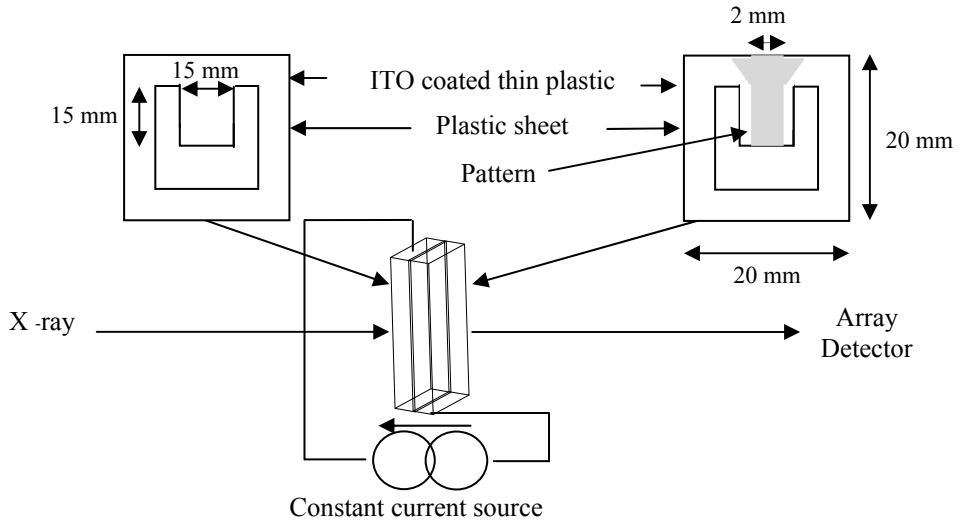

Fig. 1. Diagram illustrated thin electrochemical cell with lined patterned ITO coated thin plastic sheet used for TRXAS measurement.

3. Results and dicussion

The real time x-rays absorption was measured for electrochemical cells during electro-deposition process with various ratios between iron and nickel ions at near Fe and Ni K-edges. The XAS spectra from Fe and Ni absorptions occur at around 7112 and 8333 eV, respectively, as demonstrated for Fe:Ni ion ratio of 50:50 in Fig. 2. It cannot observe the difference between the spectra before and after applying current. The spectra of standard Fe and Ni foils were also provided to compare with the measured cell spectra. Even the deposited alloy film can be visually seen by neck eye after applying the current, the spectra of the deposited cell cannot exhibit the feature of standard foils due to not sufficient thick film comparing to the remained metal ion absorption in electrolyte. Normally the oxidation state of metal ion can be identified by the shift of absorption edge such as changing from Fe(II) in solution to Fe(0) in deposited foil. This feature can be observed if the absorption mass is enough.

In order to investigate the XAS detail of electrochemical cells at various metal ion ratios, the absolute edge jump intensity was examined for all ion ratios mixed in electrolytes for both Fe and Ni *K*-edge (Fig.3). The edge jump was derived by subtracting the absolute baseline absorption from edge absorption from the spectra before applying current. The relationship can be fitted by the linear line and the value of y-intercept can be described by the metal content from some other parts of the electrochemical cell. This linear relationship both for Fe and Ni *K*-edges indicated that the main XAS originated from the metal ions in electrolyte.

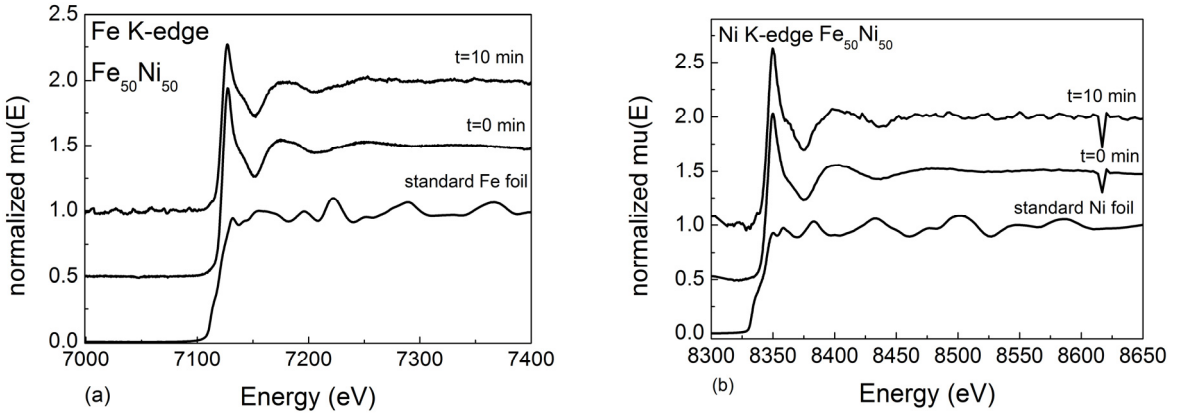

Fig. 2. Normalized x-rays absorption near a) Fe and b) Ni K-edges for electro-deposited cells with the Fe:Ni ion ratio of 50:50 at the time before applied current and after applied current for 10minutes. The absorption spectra of standard Fe and Ni foils are also provided

It can be noticed that the absolute baseline absorption intensity of deposited relative thick film becomes very weak therefore the absorption intensity difference between after and before applying current of baseline and edge absorptions was investigated as a function of Fe ion content in the electrolyte for both Fe and Ni *K*-edges. The intensity difference values calculated from baseline and edge absorptions provided the same feature. For Fe K-edge, the difference has the most negative value at about Fe:Ni ion ratio of 50:50. This can be implied that the Fe0.5Ni0.5 alloy thin film was deposited at the fastest rate and the thickest film was obtained. This can also be observed by examining the deposited film after removing the cell. This increasing of x-rays absorption can be described by x-rays absorption of thin metal solid film.

In order to investigate the XAS detail at the energy range higher than the absorption edge, the EXAFS of electrochemical cells at various metal ion ratios was examined by converting the energy to wave vector and transforming the spectra into Fourier components in R space. Fourier components in R space can be used to describe the neighbor atomic positions that scattering x-rays. Fourier components of the EXAFS spectra were calculated for collected spectra at each time step as displayed the components of some deposition time in Fig. 3 for electrochemical cell with pure nickel ion. The first peak around 1.5 A° corresponds to Ni–S bonding, whereas the second peak in 2–3.5 A° range is attributable to Ni-Ni bonding [10, 11]. It can be noticed that the second peak increased as increasing deposition time. Therefore the Fourier component can be used to indicate the formation of metal alloy film. For pure iron ion in electrochemical cell, it was hard to observe the change in Fourier component of EXAFS in R space, as illustrated in Fig. 4. The first peak around 1.5 A° corresponds to Fe–S bonding, whereas the second peak in 2–3.5 A° range is attributable to Fe–Fe bonding [11, 12]. However the relative small peak at about 0.22 nm can be observed in Fourier spectra of pure iron cell after applying current for 10 minutes. Fourier spectra for Fe K-edge do not exhibit as clear feature as that for Ni K-edge.

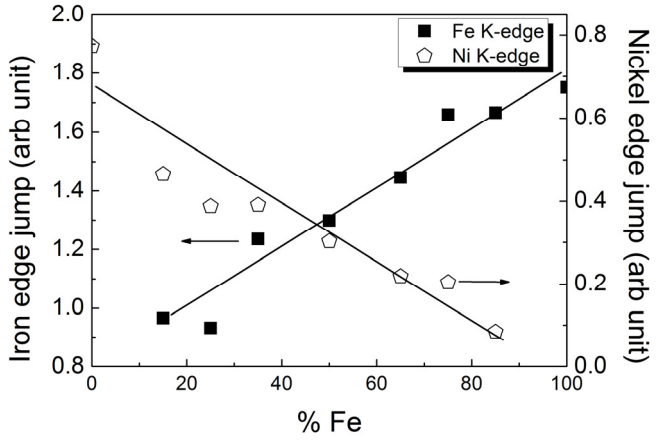

Fig. 3. Edge jump intensity as a function of percentage of iron ratio in the electrochemical cells before applying current for both Fe and Ni *K*-edges.

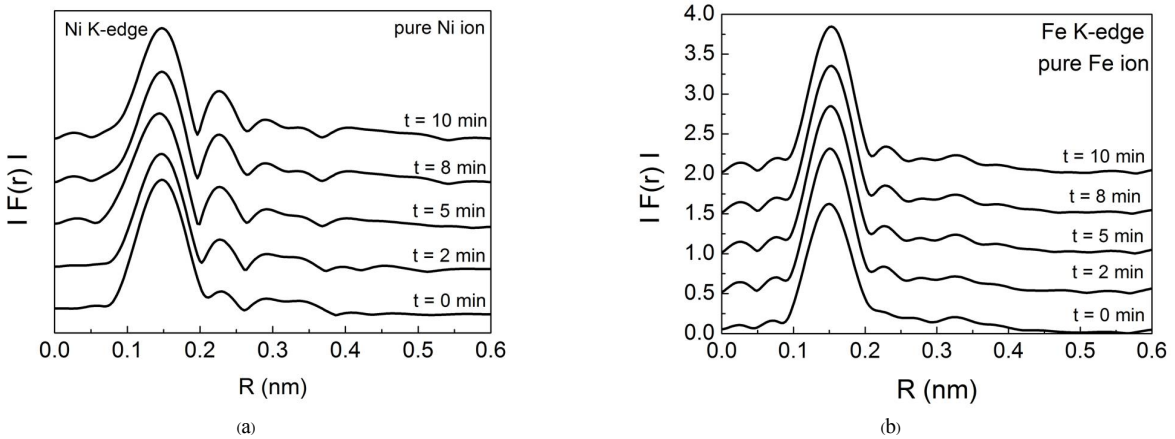

Fig. 4. Fourier component of EXAFS in R space from Ni and Fe K-edge for electrochemical cell at various deposition times

Fourier components of the first and second peaks at about 0.16 nm and 0.22 nm were investigated for each deposition time step in order to investigate the real time monitoring of metal alloy formation, as shown in Fig. 5. The relative first peak of Fourier components exhibited decreasing tend while the relative second peak showed the increasing feature. These features implied the reducing of nickel ion in electrolyte and forming of nickel metal film more than iron.

In order to monitor the electro-deposited metal alloy film formation, the relative magnitude of the Fourier second peak to the first peak was investigated at various ion ratios for both near Fe and Ni K-edges. The example for the electrochemical cell with Fe:Ni ion ratio of 50:50 was illustrated in Fig. 6. It can be seen that the relative component for Ni edge indicated the increase tend as increasing deposition time while the relative magnitude for Fe edge exhibited only slightly change. This implied that the nickel can deposit easier than that of iron

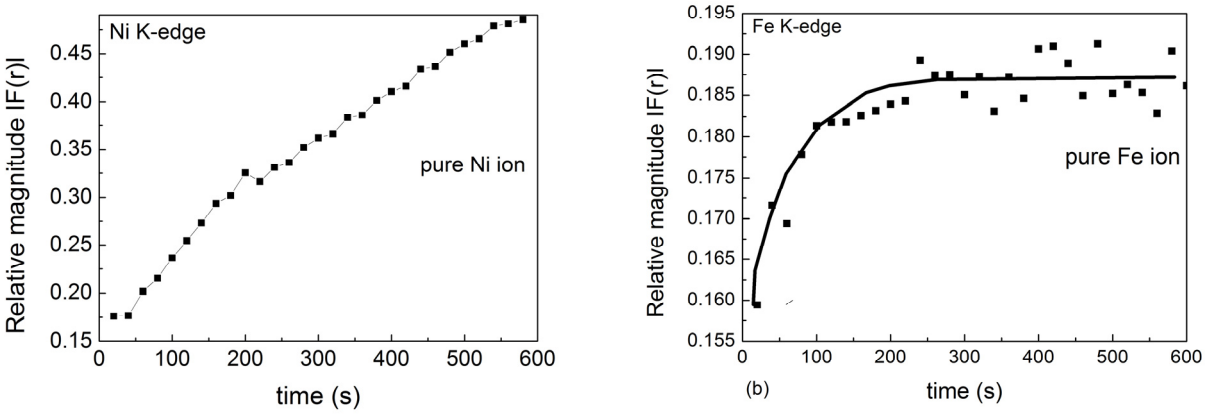

(a) (b)

Fig. 5. Relative second peak to the first peak of Fourier component of EXAFS for Ni100 and Fe100 electrochemical cell as a function of deposition time.

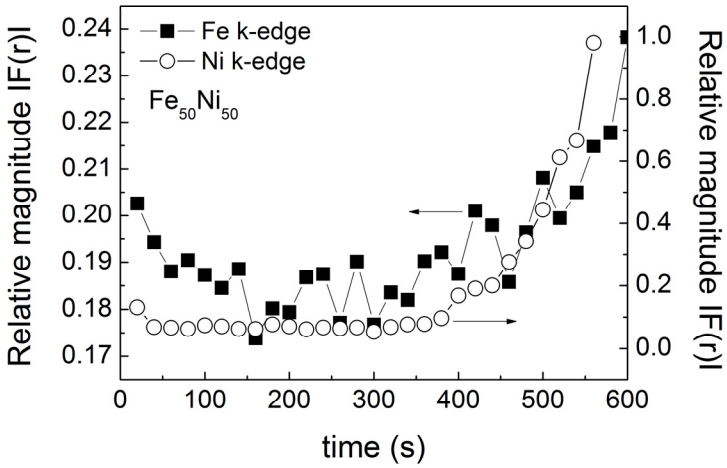

Fig. 6. Relative second peak to the first peak of Fourier component of EXAFS for Fe50Ni50 electrochemical cell as a function of deposition times at near Fe and Ni K-edges.

4. Conclusion

In this work, TRXAS is advantage for real time monitor of electro-deposition for iron-nickel thin film. Due to the sensitivity of TRXAS, the x-rays absorption edge shift cannot observe in this experiment however the modification of Fourier component from EXAFS in R space can be used to monitor the metal alloy film formation. It was found that the nickel can be observed easier than that for iron. In addition the absolute value of baseline and edge absorptions together with edge jump intensity can be used to identify the real time thickness of metal alloy films.

Acknowledgements

We would like to acknowledge beam line 2.2, Synchrotron Light Research Institute (SLRI) for TRXAS measurement. This work was partially supported by National Nanotechnology Center. The author (WI) would like to appreciate for scholarship from Development and Promotion of Science and Technology Talents (DPST).

References

[1] C. Cheung, F. Djuanda U. Erb and G. Palumbo, Nanostruct. Mater. 5 (5) (1995) 513-523.
[2] F. Czerwinski, Nanostruct. Mater. 10 (8) (1998) 1363-1369.
[3] S. Sam , G. Fortas , A. Guittoum , N. Gabouze , and S. Djebbar, Surf. Sci. 601 (2007) 4270-4273.
[4] J. Gaidelene, R. Kalendarev, A. Kuzmin, and J. Purans, Nucl. Instrum. Methods Phys. Res., Sect. A. 531 (2004) 321–326.
[5] T. Nasu, M. Sakurai , T. Kamiyama , T. Usuki, O. Uemura, and T. Yamasaki, J. Non-Cryst. Solids. (2002) 319–322.
[6] D' Addato, L. Masrassi, P Luches, and G.C. Gazzadi, , Surface Science 487 (2001) 258-266.
[7] T. Sikora, M. Jaouen, T. Girardeau, and J. Mimault, Nucl. Instrum. Methods Phys. Res., Sect. B. 111 (1996) 141- 147.
[8] Y. Poo-arporn, P. Chirawatkul, W. Saengsui, S. Chotiwan, S. Kityakarn, S. Klinkhieo, J. Hormes, and P. Songsiriritthigul, Journal of Synchrotron Radiation. 19 (2012) 937-943
[9] B. Ravel and M.Newville, Journal of Synchrotron Radiation 12. (2005) 537–541.
[10] M.E. Fleet, The crystal structure of heazlewoodite, and metallic bonds in sulfide minerals, Am. Mineral. 62 (1977) 341 -345.
[11] R.M. Lambert and G. Pacchioni, Chemisorption and Reactivity on Supported clusters and thin films, Springer. (1997).
[12] D.M.P. Mingos and G. Parkin , Metal-Metal bonding, Springer. (2010).

Applied Physics Express **5** (2012) 025203
DOI: 10.1143/APEX.5.025203

Ordering of C_{60} on One-Dimensional Template of Single-Domain Ge(110)-16×2 and Si(110)-16×2 Surfaces

Yuta Yokoyama[1,2], Asawin Sinsarp[3], Yoichi Yamada[1]*, Hidehito Asaoka[2], and Masahiro Sasaki[1]

[1]*Institute of Applied Physics, University of Tsukuba, Tsukuba, Ibaraki 305-8573, Japan*
[2]*Quantum Beam Science Directorate, Japan Atomic Energy Agency, Tokai, Ibaraki 319-1195, Japan*
[3]*Department of Physics, Faculty of Science, Mahidol University, Ratchathewi, Bangkok 10400, Thailand*

Received January 10, 2012; accepted January 27, 2012; published online February 13, 2012

We demonstrated the ordering of C_{60} in one dimension by using Ge(110)-16×2 and Si(110)-16×2 single-domain surfaces as one-dimensional templates. We achieved the formation of one-dimensional order of C_{60} molecules along the atomic rows of the Ge(110)-16×2 surface where surface diffusion of C_{60} is activated at room temperature. In contrast, the substantial reactivity of the Si(110)-16×2 surface limited the diffusion of adsorbed C_{60}, resulting in random adsorption even at elevated temperatures. © 2012 The Japan Society of Applied Physics

Formation of molecular nanowires by means of molecular self-assembly on the surfaces of substrates is one of the key technologies in molecular electronics, where the template effect of anisotropic surface structures such as step edges for growing molecules in one dimension plays an important role.[1)] Si(110)-16×2- and Ge(110)-16×2-reconstructed surfaces have a very anisotropic, quasi one-dimensional structure, which has been regarded as a good template for growing nanowires. In fact, Si(110)-16×2 has been used to form nanowires of such as silicides,[2–4)] metal or semiconductor elements.[5,6)] However, many of them involve further rearrangements of surface atoms resulting in the formation of "embedded" nanowires, whose mechanism does not seem to be effective in the synthesis of molecular nanowires. In order to grow the molecular nanowires on Si(110)-16×2 or Ge(110)-16×2, the topmost atomic structure of the 16×2 structure showing strong one dimensionality should be utilized; however, this has not been achieved so far.

Two major problems have hindered the synthesis of molecular nanowires on the 16×2-reconstructed surface: (1) the inhomogeneity of the surface structure due to multiple domains reduces the quality of the template effect; (2) the strong reactivity of the surface electronic structure limits molecular self-assembly. However, recent progress in understanding and controlling this surface seems to have overcome these difficulties. On Si(110), the well-defined single-domain of the 16×2 reconstruction has been recently realized.[7,8)] The single domain of the 16×2 reconstruction has a simplified morphology of densely packed parallel atomic steps running along one particular direction and exhibits strong one dimensionality. This offers an attractive one-dimensional template surface. In addition, detailed angle-resolved photoemission spectroscopy (ARPES)[9)] and scanning tunneling microscopy (STM) studies[10,11)] have revealed the dispersion and binding energies, as well as the precise spatial distribution of the surface electronic states of Si(110)-16×2. These studies have largely helped in understanding the chemical properties of the surface and deducing a sophisticated model of the surface atomic structure. Furthermore, recent reports on hydrogen and water adsorption on Si(110)-16×2[12)] have suggested promising strategies to grow molecular nanowires. Surprisingly, Si(110)-16×2 was found to be quite inert against atomic hydrogen exposure.[12)] The inertness of the surface is attractive because the enhancement of molecular diffusion is expected. On the other hand, distinct chemical adsorption sites for dissociated water molecules were found (U3 and L3 in ref. 12, hereafter referred to as U3), which are periodically arranged along the step edges of the 16×2 reconstruction. By utilizing the enhanced diffusion and selective adsorption to the specific sites at the step edges on the single-domain of the 16×2 reconstruction, ordering of the organic molecules in one dimension may be achieved.

In this article, using the single-domain of Ge(110)-16×2, we showed that the above strategy is successful. We found that the single domain of the 16×2 reconstruction of the Ge(110) surface can be formed in the same manner as that in the case of Si(110)-16×2. The Ge(110)-16×2 surface was found to be even less reactive than the Si(110)-16×2 surface, facilitating molecular diffusion and stabilization at distinct stable adsorption sites along step edges. This in fact enabled us to achieve one-dimensional ordering of C_{60}. Subsequently, we discuss two key points that help in realizing the one-dimensional ordering of C_{60} molecules: (1) the preparation of the single-domain of the 16×2 structure on Ge(110) as well as Si(110), and (2) the utilization of molecular diffusion on both templates.

Here, we briefly discuss the first key point. The fabrication of the single-domain of Ge(110)-16×2 is similar to that of Si(110)-16×2. We used a specimen of moderately doped n-type Ge(110) with approximately 0.1 Ω cm resistivity. The wafers were cut into a rectangular shape ($2 \times 8\,mm^2$), with their long side set along the [1$\bar{1}$2] direction. Surface cleaning was performed with Ar-ion sputtering and direct current (DC) heating. We will report the details of the preparation method elsewhere.[13)] The obtained single domain of the 16×2 reconstruction on Ge(110) is shown in Fig. 1(a). In Fig. 1(b), single-domain Si(110)-16×2 prepared according to the procedure reported in ref. 7 is also shown. It can be seen that the overall appearance of the surface structure of Ge(110)-16×2 is quite similar to that of Si(110)-16×2. The low-energy electron diffraction (LEED) images obtained for both surfaces (not shown) were in agreement with that in previous reports.[14,15)] The period and corrugation due to the atomic rows were found to be approximately 5 and 0.2 nm, respectively, for both surfaces. The insets in Figs. 1(a) and 1(b) show the atomically resolved STM images obtained in the filled states imaging. The atomic contrasts of Ge(110) and Si(110) appear very similar and agree with previous

*E-mail address: yamada@bk.tsukuba.ac.jp

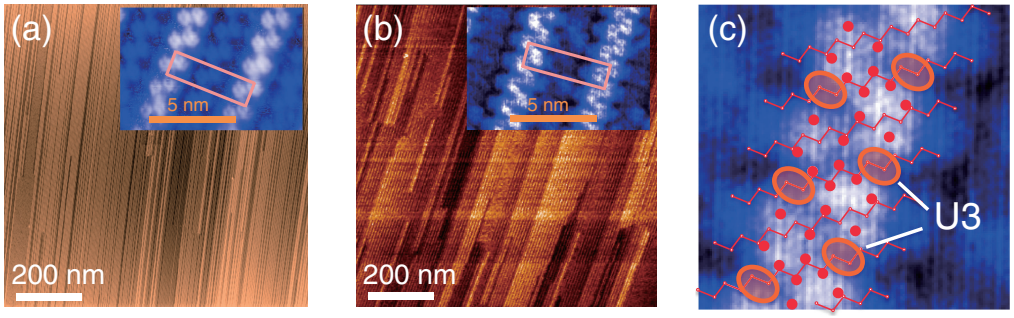

Fig. 1. $1 \times 1\,\mu m^2$ STM images of (a) Ge(110)-16×2 single domain and (b) Si(110)-16×2 single domain. In the inset, magnified images showing atomic contrast are shown. Unit cells of the 16×2 structures are indicated with orange parallelograms. STM images [(a) and (b)] are obtained with a sample bias voltage of −1.0 V and tunneling current of 0.3 nA. (c) Magnified image of the upper terrace of the Si(110)-16×2 surface. Atomic structures (large and small red circles) as well as the position of surface localized U3 states (orange hutched ovals) are indicated according to refs. 11 and 12. Larger red circles represent pentagonal adatoms, which are constructed on the basis of ref. 11. Small circles represent Si atoms in the second layer.

studies.[10,11,16] The details of the atomic structure and positions of the surface-localized electronic states, which are responsible for the water adsorption (U3 state)[12] in Si(110), are provided in Fig. 1(c). Quantitative comparison of the geometric and electronic structures based on the STM and STS measurements will be reported elsewhere.[13] It should be noted here that while these two surfaces exhibit very similar surface structures, their electronic properties are possibly different, resulting in differences in molecular adsorptions.

Next, we argue about the second key point, i.e., molecular diffusion and self-assembly on the Ge(110)-16×2 and Si(110)-16×2 templates, by observing the adsorption of C_{60}. On Ge(110)-16×2, it is clearly found that most C_{60} molecules are adsorbed on the step edges at room temperature, as shown in Fig. 2(a). This observation is in strong contrast to that of Si(110)-16×2,[17] where rather random adsorption of C_{60} has been reported. The molecules at the step edges of Ge(110)-16×2 can then order in one dimension with increasing amount of C_{60} molecules. Indeed, it was found that the numbers of dimers, trimers, tetramers, etc., increased with increasing coverage, as shown in Fig. 2(b). These observations clearly indicate that the most stable adsorption sites for C_{60} molecules exist at the step edges and that the molecules can diffuse over large distances to reach the most stable adsorption sites on Ge(110) even at room temperature. Figure 2(c) shows a precise STM scan around the adsorption site of single C_{60} molecules with enhanced contrast for the upper terrace of the 16×2 structure. It is clearly observed that the C_{60} molecules are adsorbed between the zigzag contrasts of the pairs of pentagons. Note that most C_{60} molecules, including those forming nanowires, were adsorbed in the same configuration. The adsorption position of C_{60} on Ge(110)-16×2 is similar to that of water molecules on Si(110)-16×2, at which the so-called U3 surface states are localized[12] as shown in Fig. 1(c). Thus, the observations suggest that a similar state (U3-like state) also exists in Ge(110)-16×2 and offers stable adsorption sites for C_{60} molecules. It should be also noted that there exist small fraction of so-called (17, 15, 1) type steps in the 16×2 region that may have different atomic structure.[15,16,18] We found that the adsorption of C_{60} onto (17, 15, 1) type steps is very similar to that on the 16×2 region. However, systematic studies may be required to elucidate the difference in reactivity of these two structures more precisely.

It is found that the intermolecular distance in the C_{60} chains shown in Fig. 2(b) is approximately 1.4 nm, which is much longer than the intermolecular distance of approximately 1.0 nm normally found in the hexagonal close-packed C_{60} islands on metal substrates.[19] This is because the molecules are stabilized at the U3-like state, which is arranged with a separation of approximately 1.4 nm along the step edge, as shown in Fig. 1(c). This observation suggests that the binding energy of C_{60} to the U3-like state is larger than that of intermolecular adhesion. Thus, the formation of C_{60} chains on Ge(110)-16×2 is somewhat different from the pure molecular self-organization commonly seen at step edges on metal substrates.[20] In contrast, the strong template effect found on the Ge(110)-16×2 surface, i.e., the nearly

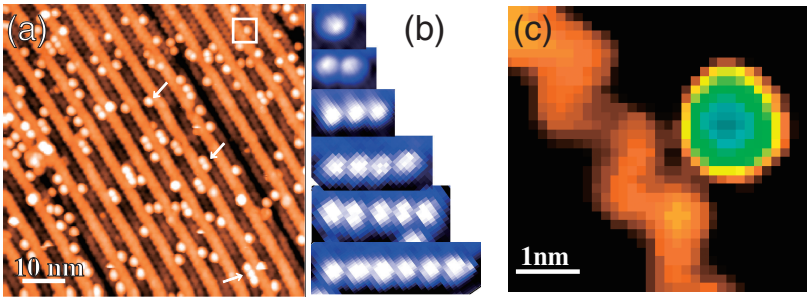

Fig. 2. (a) $50 \times 50\,nm^2$ STM image of Ge(110)-16×2 covered with a small amount of C_{60} molecules. Arrows indicate the monomer, dimer, and trimer of C_{60} molecules. (b) STM images of C_{60} nanowires formed at the step edges. (c) Magnified STM image of C_{60} adsorbed at the step edge of Ge(110)-16×2. The scan area is indicated by a white square in (a).

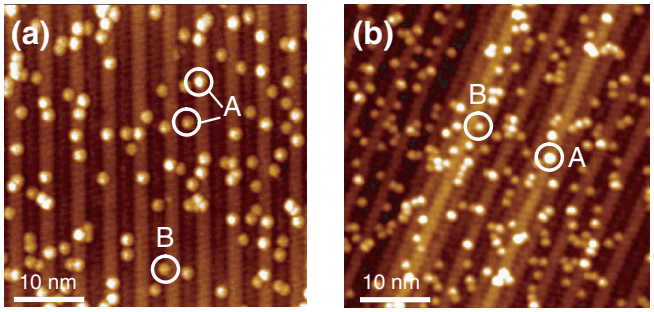

Fig. 3. (a) $50 \times 50\,nm^2$ STM image of Si(110)-16×2 covered with a small amount of C_{60} molecules, prepared at room temperature. (b) $50 \times 50\,nm^2$ STM image of Si(110)-16×2 covered with a small amount of C_{60} molecules, prepared at a surface temperature of 200 °C.

perfect selective adsorption to the well-aligned U3-like states, can result in the formation of rather well-defined, one-dimensional ordering of organic molecules. Thus, it can be concluded that the strategy to grow molecular nanowires discussed in the beginning is successful on Ge(110)-16×2. However, there exist some parameters to be optimized in order to synthesize well-ordered functional nanowires on this template. It was found that the population of monomer is still the largest (approximately 49%) even around the monolayer region, suggesting that the diffusion of C_{60} is still not very efficient at room temperature. The surface temperature should thus be optimized to control the length distribution of nanowires. It is also noted that since C_{60} possesses considerably strong intermolecular adhesion, additional adsorption onto the molecular wires occurs at higher C_{60} concentrations, making it difficult to form a regular array of long nanowires. Hence, it is important to control molecular adhesion in order to form further well-defined organic nanowires. Furthermore, the present C_{60} nanowires are, most likely, not conducting due to elongated intermolecular distance. It is suggested that, in order to achieve conducting wires, the size of the molecules should be optimized.

In contrast to the case of Ge(110), C_{60} deposition on Si(110)-16×2 is known to result in disordered monolayers.[17] Indeed, only weak preferential adsorption to the step edges was observed in the STM image shown in Fig. 3(a). In the STM image, adsorptions at the center of the upper or lower terrace (marked as "A"), at the step edge ("B"), and at the position between them are found. It is seen that the populations of the adsorption on the "A" site were much larger (approximately 80%) than those on "B" (approximately 20%), which is different from the case of Ge(110)-16×2. Increasing the coverage of C_{60} resulted in increasing disorder, which agrees with the previous reports.[17] A similar tendency was found in other molecules such as Cu-phthalocyanine and pentacene and coronene molecules (not shown). The disordering of the molecular layers on the Si(110)-16×2 may occur because of the strong interaction between the Si adatoms and adsorbed molecules, which hinders molecular diffusion. To facilitate the molecular diffusion, we aimed to activate the molecular diffusion by increasing the substrate temperature. We deposited C_{60} on the surface at 200 °C, and the result is shown in Fig. 3(b). It is found that the population of adsorption sites at the step edge ("B") clearly increased up to approximately 70%. The molecules at the step edges were found to adsorb in the same configuration as that shown in Fig. 2(c). This suggests that the most stable adsorption site of C_{60} on Si(110)-16×2 is also at the U3 state at the step edge and that stable adsorption becomes possible owing to enhanced diffusion at elevated surface temperatures. However, the ordering of C_{60} molecules on Si(110) was still less perfect and the population of the molecules residing at other adsorption sites was still noticeable, even with preparation at temperatures up to 600 °C. These observations reveal that diffusion of C_{60} is still insufficient on the Si surface. This reflects either the stronger Si-molecule interaction or the presence of extra adsorption sites ("A" sites) that do not exist on Ge(110)-16×2. The clear difference between the adsorptions of C_{60} on Ge(110)-16×2 and Si(110)-16×2 reveals the difference in the electronic structure, whereas the detection of the same adsorption sites both on Ge(110)-16×2 and Si(110)-16×2 indicates, to a certain extent, the similarity of the surface electronic structures. These results call for further detailed studies including theoretical calculations in order to elucidate the nature of these unique surfaces, which will be valuable for the further utilization of these template surfaces.

In conclusion, we have prepared well-defined single domains of Ge(110)-16×2 and Si(110)-16×2. On Ge(110)-16×2, where molecular diffusion is activated even at room temperature, most of the C_{60} molecules were adsorbed at particular positions (U3-like state), realizing the one-dimensional order of the C_{60} molecules. On Si(110)-16×2, where molecular diffusion is limited, the alignment of C_{60} to the stable adsorption sites (U3) required elevated surface temperatures. The selective adsorption onto the U3 state realized in Ge(110)-16×2 may be universally utilized to grow molecular nanowires. The present results suggested that the parameters such as the molecular size, the intermolecular cohesion and the surface temperature should be optimized in order to achieve well-ordered functional nanowires on this template.

Acknowledgments We are grateful to Professor K. Miki (NIMS, Japan) for fruitful discussions. This research has been supported in part by Grants-in-Aid for Scientific Research B (20310064, H.A.) and for Young Scientists (20760028, Y.Y.) from the Japan Society for the Promotion of Science (JSPS). A.S. would like to thank the support of the Follow-up Research Fellowship for Fiscal 2011 from the Japan Students Support Organization (JASSO) and the Research Grant for New Scholars contract number MRG5380127 from the Commission on Higher Education and the Thailand Research Fund (TRF).

1) J. V. Barth *et al.*: Nature **437** (2005) 671.
2) Z. He *et al.*: Appl. Phys. Lett. **83** (2003) 5292.
3) Z. He *et al.*: Phys. Rev. Lett. **93** (2004) 256102.
4) S. Liang *et al.*: Appl. Phys. Lett. **88** (2006) 113111.
5) M. Jałochowski and E. Bauer: Surf. Sci. **480** (2001) 109.
6) T. An *et al.*: Surf. Sci. **576** (2005) 165.
7) Y. Yamada *et al.*: Phys. Rev. B **76** (2007) 153309.
8) Y. Yamada *et al.*: Phys. Rev. B **77** (2008) 153305.
9) K. Sakamoto *et al.*: Phys. Rev. B **79** (2009) 045304.
10) T. An *et al.*: Phys. Rev. B **61** (2000) 3006.
11) M. Setvín *et al.*: Phys. Rev. B **84** (2011) 115317.
12) M. Setvín *et al.*: Phys. Rev. B **82** (2010) 125421.
13) Y. Yamada *et al.*: in preparation.
14) Y. Yamamoto *et al.*: Jpn. J. Appl. Phys. **25** (1986) L331.
15) H. Noro and T. Ichikawa: Jpn. J. Appl. Phys. **24** (1985) 1288.
16) T. Ichikawa: Surf. Sci. **544** (2003) 58.
17) Y.-R. Ma *et al.*: Surf. Sci. **397** (1998) 421.
18) T. Ichikawa: Surf. Sci. **560** (2004) 213.
19) Y. Yamada *et al.*: Jpn. J. Appl. Phys. **50** (2011) 08LB06.
20) N. Neel *et al.*: Appl. Phys. Lett. **88** (2006) 163101.